

Spatial and Wavelength Division Joint Multiplexing System Design for Visible Light Communications

Cheng Chen, *Member, IEEE*, Shenjie Huang, *Member, IEEE*,
Iman Tavakkolnia, *Member, IEEE*, Majid Safari, *Senior Member, IEEE*,
and Harald Haas, *Fellow, IEEE*

Abstract

The low-pass characteristics of front-end elements including light-emitting diodes (LEDs) and photodiodes (PDs) limit the transmission data rate of visible light communication (VLC) and Light Fidelity (LiFi) systems. Using multiplexing transmission techniques, such as spatial multiplexing (SMX) and wavelength division multiplexing (WDM), is a solution to overcome bandwidth limitation. However, spatial correlation in optical wireless channels and optical filter bandpass shifts typically limit the achievable multiplexing gain in SMX and WDM systems, respectively. In this paper, we consider a multiple-input multiple output (MIMO) joint multiplexing VLC system that exploits available degrees-of-freedom (DoFs) across space, wavelength and frequency dimensions simultaneously. Instead of providing a new precoder/post-detector design, we investigate the considered joint multiplexing system from a system configuration perspective by tuning system parameters in both spatial and wavelength domains, such as LED positions and optical filter passband. We propose a novel spatial clustering with wavelength division (SCWD) strategy which enhances the MIMO channel condition. We propose to use a state-of-the-art black-box optimization tool: Bayesian adaptive direct search (BADs) to determine the desired system parameters, which can significantly improve the achievable rate. The extensive numerical results demonstrate the superiority of the proposed method over conventional SMX and WDM VLC systems.

Cheng Chen, Iman Tavakkolnia and Harald Haas are with the Department of Electrical and Electrical Engineering, the University of Strathclyde, Glasgow, Scotland, UK.

Shenjie Huang and Majid Safari are with the institute for Digital Communications, School of Engineering, University of Edinburgh, Edinburgh, Scotland, UK.

Harald Haas acknowledges the financial support from the Wolfson Foundation, the Royal Society, and Engineering and Physical Sciences Research Council (EPSRC) under Established Career Fellowship grant EP/R007101/1.

Index Terms

Visible light communication, optical wireless communication, multiple-input multiple-output, orthogonal frequency division multiplexing, spatial multiplexing, wavelength division multiplexing.

I. INTRODUCTION

With the development of information technology, an increasing number of machine-type devices, wireless sensors and cloud services are deployed, which further increases the demand on wireless network capability [1]. To meet the need of future wireless services, various new technologies for high speed wireless transmission have been proposed. visible light communication (VLC) and light fidelity (LiFi) are among potential candidates [2]. Apart from the use of the license-free optical spectrum and physical layer security feature, VLC and LiFi can deliver multi-Gbps transmission data rate [3]. A major challenge of developing high performance VLC and LiFi systems is the limited modulation bandwidth of light-emitting diodes (LEDs) and photodiodes (PDs). One of the solutions is to develop optical front-ends with a much wider bandwidth, such as GaN-based micro-LEDs [4]. An alternative solution is to use spatial multiplexing (SMX) or wavelength division division (WDM) techniques to transmit data with multiple parallel channels, which can significantly boost the aggregate data rate without expanding the modulation bandwidth.

Several early studies on SMX with/without precoding/post-detection have been reported in [5]–[7]. To include the frequency-domain characteristics, VLC systems with multiple-input multiple-output (MIMO)-orthogonal frequency division multiplexing (OFDM) have been investigated in [8], [9]. In addition, a coherent LiFi system with SMX has been considered in a recent study [10]. Regarding research on WDM-based VLC systems, many successful experimental demonstrations were reported in the literature [11], [12]. An analytical work shows that the achievable data rate is limited by inter-channel crosstalk when a large number of wavelength divisions are used [13]. In order to mitigate the crosstalk, the usage of signal processing in MIMO systems have been proposed in a few studies [14], [15], where the WDM channels are treated as a colour MIMO channel matrix and precoding/post-detection processes are used to diagonalise the multiplexing channel matrix. A recent study shows that it is possible to implement a WDM system without using optical filters [16].

A. Related research

Regarding the combination of SMX and WDM VLC systems, MIMO-VLC systems with multi-colour LEDs have been considered to use degree-of-freedom (DoFs) in both dimensions [17], [18]. These studies have proposed signal processing techniques such as optimal precoder designs under lighting constraints [17] or a chromaticity-adaptive generalised spatial modulation scheme [18]. In these studies, advanced signal processing techniques are generally designed to improve communication performance with a given set of system parameters. Alternatively, the performance of VLC systems can also be improved by changing system configurations, where key system parameters, such as LED position or optical filter passband, are carefully selected so that the probability of improved channel quality is increased. Several studies in multi-cell LiFi systems investigated the optimal system configurations in terms of access points (APs) spatial deployment and LED parameters so that the system reliability, spectral efficiency or energy efficiency is maximised [19]–[22]. Regarding the research on system configurations in VLC MIMO systems, angular diversity receivers (ADRs), mirror diversity receiver and irregular PD configurations are investigated to improve MIMO channel condition [23]–[25]. System configurations of wavelength domain parameters in WDM VLC systems have been investigated in [13], [26]. Nevertheless, the above studies consider system configurations with only a few parameters in either the spatial or wavelength domain.

B. Motivation and contributions

Due to significant spatial correlation, the number of parallel channels in SMX VLC systems is limited [25]. On the other hand, it has been shown that the passband of a thin film optical filter will shift to shorter wavelengths when the light incident angle is greater than 0° , which causes a severe wavelength mismatch in a WDM VLC system [26]. By considering a spatial and wavelength division joint multiplexing VLC system, the MIMO channel with severe spatial correlation can be decorrelated by the wavelength domain features. In addition, the excessive inter-colour interference in wavelength domain due to aforementioned passband shift issue can be mitigated by MIMO precoding and post-processing blocks. Consequently, the resultant number of parallel channels in joint multiplexing system can be increased and the corresponding achievable rates can be improved. Despite the performance improvement from the novel signal processing techniques, the combining features in spatial and wavelength domains have not been comprehensively investigated in [17], [18]. The research findings in [19]–[26] also demonstrate

the importance of system configuration in VLC/LiFi systems, which has not been explored in a spatial and wavelength domain joint multiplexing VLC system yet. Furthermore, it is complicated to design a VLC multiplexing system using both spatial and wavelength domain features efficiently. In this paper, a MIMO-OFDM spatial and wavelength division joint multiplexing VLC system is thoroughly studied from a system configuration perspective. To evaluate the impact of various parameters, a detailed framework of a MIMO-OFDM joint multiplexing VLC system is established considering the characteristics in the spatial, wavelength and frequency domains, which is unavailable in the literature. Based on the developed framework, the achievable rates with various system configurations are evaluated and compared. In particular, a unique spatial clustering with wavelength division (SCWD) configuration strategy is proposed which can achieve higher achievable rates compare to the other benchmark strategies. Furthermore, a Bayesian adaptive direct search (BADs) black-box optimisation tool has been used to search for system parameters that offer additional performance improvement. Compared to our previous study [27], a more detailed system model and more scenarios with practical concerns such as random user position/orientation are considered. The contributions of this study are summarised as follows:

- A detailed framework is established for characterising VLC MIMO-OFDM joint multiplexing systems over space, wavelength and frequency domains. This framework allows researchers to evaluate the performance of a joint multiplexing system with a specific system configuration.
- The system configurations of the considered VLC MIMO-OFDM joint multiplexing system are thoroughly investigated with random user position and device orientation. Both empirical parameter selections and parameter searching based on BADs algorithm are considered.
- Based on the idea of ‘division in either the spatial or wavelength domain’, a SCWD strategy is proposed to efficiently use the DoF in both spatial and wavelength domains. The performance of the joint multiplexing systems using the SCWD strategy is compared with benchmark systems, which shows the superiority of the joint multiplexing system over SMX and WDM techniques in terms of achievable rate.
- It has been found that systems with the SCWD strategy are superior to SMX and WDM when two specific conditions are fulfilled: 1. When the achievable rates of SMX and WDM are similar (with the same number of elements); 2. When the multiplexing gain

improvement from excessively increasing numbers of LEDs/PDs is saturated for SMX and WDM techniques. Insights into system configuration strategies and solutions are presented.

The remainder of this paper is arranged as follows. Section II presents the considered MIMO-OFDM system model. The MIMO channel model considering characteristics in space, wavelength and frequency domains are introduced in Section III. The system configuration of the joint multiplexing system is thoroughly investigated in Section IV. The conclusions are drawn in Section V.

II. MIMO-OFDM SYSTEM MODEL

In this section, a conventional MIMO-OFDM VLC system model based on DC-biased optical (DCO)-OFDM is considered [8]. A block diagram of the system is shown in Fig. 1. Assuming there are N_t LEDs and N_r PDs, the maximum supported number of data streams will be $I \leq \min(N_t, N_r)$. Considering a K -point fast Fourier transform (FFT) operation, the number of subcarriers carrying information bits is $\tilde{K} = K/2 - 1$. Firstly, a modulation block maps information bits to M -ary quadrature amplitude modulation (QAM) symbols. Then, after a power control module and a precoding module, the signal vector on the k th subcarrier can be represented by:

$$\mathbf{X}_k = \mathbf{F}_k \mathbf{Q}_k^{1/2} \mathbf{S}_k, \text{ for } k = 1, 2, \dots, \tilde{K}, \quad (1)$$

where $\mathbf{S}_k \in \mathbb{C}^{I \times 1}$ is the modulated symbol vector with unit variance; $\mathbf{Q}_k^{1/2} \in \mathbb{R}^{I \times I}$ is power control diagonal matrix and $\mathbf{F}_k \in \mathbb{C}^{N_t \times I}$ is a precoding matrix, which must be a unity matrix. Note that the QAM symbol on the k th subcarrier of the i th data stream is defined as $S_i[k]$, which is also the i th element of \mathbf{S}_k . Thus, the signal value on the k th subcarrier for the n_t th LED can be written as:

$$X_{n_t}[k] = \sum_{i=1}^I F_{n_t,i}[k] \sqrt{q_i[k]} S_i[k], \quad (2)$$

where $\sqrt{q_i[k]}$ is the (i, i) -th entry of $\mathbf{Q}_k^{1/2}$ and $F_{n_t,i}[k]$ is the (n_t, i) -th entry of \mathbf{F}_k . To guarantee a real-value time-domain signal, the Hermitian symmetry condition must be fulfilled, which requires: $X_{n_t}[0] = X_{n_t}[K/2] = 0$ and $X_{n_t}[k] = X_{n_t}^*[K - k]$ for $k = K/2 + 1, K/2 + 2, \dots, K - 1$. Next, the frequency-domain signal is converted to time-domain for transmission by using an inverse fast Fourier transform (IFFT) operation:

$$x_{n_t}[n] = \frac{1}{\sqrt{K}} \sum_{k=0}^{K-1} X_{n_t}[k] e^{\frac{2\pi n k j}{K}}, \quad (3)$$

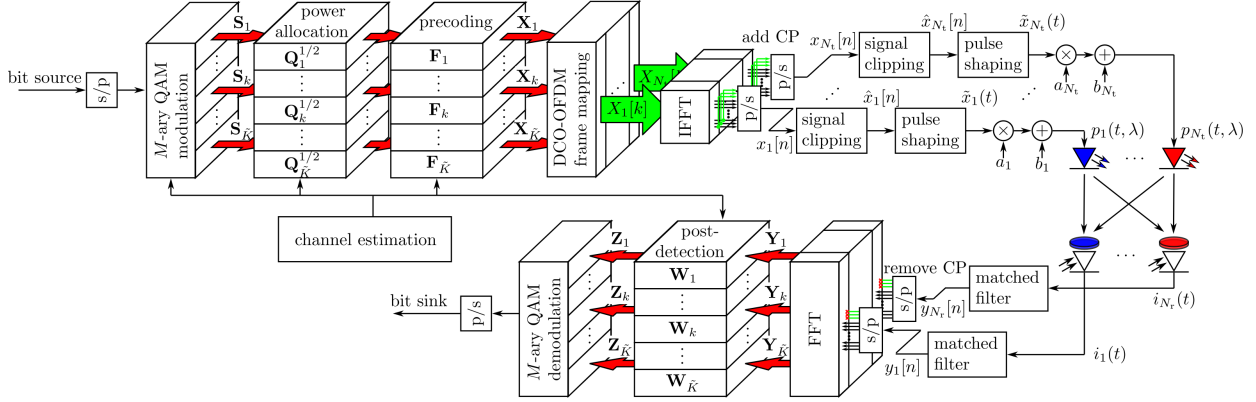


Figure 1: Block diagram of a MIMO-OFDM VLC system based on DCO-OFDM.

where $j = \sqrt{-1}$ is the imaginary number. Due to the limited dynamic range of each LED, we normalise and constrain the signal variance not to be greater than unity: $\mathbb{E}\{x_{n_t}^2[n]\} \leq 1$, where $\mathbb{E}\{\cdot\}$ refers to the expectation operator. Note that the optical power constraint is considered in Section III-A. To avoid inter-frame interference and inter-symbol interference (ISI), a cyclic prefix (CP) is added to the beginning of each time-domain OFDM frame. After the precoding and IFFT operations, a clipping operation is enforced to limit the signal peak-to-average power ratio (PAPR):

$$\hat{x}_{n_t}[n] = \begin{cases} \kappa_t & : x_{n_t}[n] \geq \kappa_t \\ x_{n_t}[n] & : \kappa_b < x_{n_t}[n] < \kappa_t \\ \kappa_b & : x_{n_t}[n] \leq \kappa_b \end{cases}, \quad (4)$$

where κ_t and κ_b are the top and bottom clipping levels. According to the Busgang theorem, the non-linear clipping operation can be approximated by:

$$\hat{x}_{n_t}[n] = \eta x_{n_t}[n] + \mathfrak{n}_{n_t}^{\text{clip}}[n], \quad (5)$$

where η is the clipping attenuation factor and $\mathfrak{n}_{n_t}^{\text{clip}}[n]$ is the clipping noise at the n_t th LED [28] which follows a normal distribution with a zero mean and a variance of σ_{clip}^2 . The value of $\mathfrak{n}_{n_t}^{\text{clip}}[n]$ and σ_{clip}^2 can be calculated analytically [29]. Then, the clipped electric signal is converted to an optical signal and launched to the optical wireless channel. At the receiver side, a fraction of the optical signals are detected by the PDs. The detected signal by the n_r th PD can be calculated as:

$$y_{n_r}[n] = \mathfrak{n}_{n_r}^{\text{rx}}[n] + \sum_{n_t=1}^{N_t} \hat{x}_{n_t}[n] \otimes h_{n_r, n_t}[n], \quad (6)$$

where $\mathbf{n}_{n_r}^{\text{rx}}[n]$ is the receiver noise, $h_{n_r, n_t}[n]$ is the discrete channel impulse response between the n_r -th PD and n_t -th LED and \otimes refers to the convolution operator. The receiver noise follows a normal distribution with a zero mean and a variance of $\sigma_{\text{rx}, n_r}^2$. The considered receiver noise is composed of the shot noise and thermal noise. After the reception of the signal, the CP is removed. The time-domain signal is converted back to the frequency-domain using the FFT operation as:

$$Y_{n_r}[k] = \frac{1}{\sqrt{K}} \sum_{k=0}^{K-1} y_{n_r}[n] e^{-\frac{2\pi n k j}{K}}. \quad (7)$$

The addition of CPs leads to the circular convolution relationship between the time-domain signal and the channel impulse response. This circular convolution can be converted to a multiplication relationship in the frequency-domain. Therefore, the conversion between $Y_{n_r}[k]$ and $X_{n_t}[k]$ can also be evaluated in the frequency-domain directly. The received signal vector on the k th subcarrier $\mathbf{Y}_k \in \mathbb{C}^{N_r \times 1}$ can be calculated by:

$$\mathbf{Y}_k = \mathbf{H}_k (\eta \mathbf{X}_k + \mathbf{E}_k) + \mathbf{N}_k, \quad (8)$$

where $\mathbf{H}_k \in \mathbb{C}^{N_r \times N_t}$ is the frequency-domain channel matrix, $\mathbf{E}_k \in \mathbb{C}^{N_t \times 1}$ is the frequency-domain clipping noise vector and $\mathbf{N}_k \in \mathbb{C}^{N_r \times 1}$ is the frequency-domain receiver noise vector. The (n_r, n_t) -th entry of \mathbf{H}_k is denoted as $H_{n_r, n_t}[k]$, the n_t -th entry of \mathbf{E}_k is denoted as $N_{n_t}^{\text{clip}}[k]$ and the n_r -th entry of \mathbf{N}_k is denoted as $N_{n_r}^{\text{rx}}[k]$. In addition, $H_{n_r, n_t}[k]$, $N_{n_t}^{\text{clip}}[k]$ and $N_{n_r}^{\text{rx}}[k]$ are FFT of $h_{n_r, n_t}[n]$, $\mathbf{n}_{n_t}^{\text{clip}}[n]$ and $\mathbf{n}_{n_r}^{\text{rx}}[n]$, respectively. Finally, a MIMO post-detection matrix $\mathbf{W}_k \in \mathbb{C}^{I \times N_r}$ is used to retrieve the transmitted data symbol vectors:

$$\mathbf{Z}_k = \mathbf{W}_k \mathbf{Y}_k = \eta \mathbf{W}_k \mathbf{H}_k \mathbf{F}_k \mathbf{Q}_k^{1/2} \mathbf{S}_k + \mathbf{W}_k \mathbf{H}_k \mathbf{E}_k + \mathbf{W}_k \mathbf{N}_k. \quad (9)$$

Thus, the data symbol of the i th data stream on the k th subcarrier can be written as:

$$\begin{aligned} Z_i[k] &= \eta \sum_{n_r=1}^{N_r} \sum_{n_t=1}^{N_t} W_{i, n_r}[k] H_{n_r, n_t}[k] F_{n_t, i}[k] \sqrt{q_i[k]} S_i[k] + \sum_{n_r=1}^{N_r} \sum_{n_t=1}^{N_t} W_{i, n_r}[k] H_{n_r, n_t}[k] N_{n_t}^{\text{clip}}[k] \\ &+ \eta \sum_{n_r=1}^{N_r} \sum_{n_t=1}^{N_t} \sum_{\hat{i}=1, \hat{i} \neq i}^I W_{i, n_r}[k] H_{n_r, n_t}[k] F_{n_t, \hat{i}}[k] \sqrt{q_{\hat{i}}[k]} S_{\hat{i}}[k] + \sum_{n_r=1}^{N_r} W_{i, n_r}[k] N_{n_r}^{\text{rx}}[k], \end{aligned} \quad (10)$$

where $W_{i, n_r}[k]$ is the (i, n_r) -th entry of \mathbf{W}_k , the first term on the right-hand side of the equality is the desired signal, the second term is the equivalent clipping noise, the third term is the interference from other multiplexing channels and the last term corresponds to the equivalent

receiver noise. Therefore, the corresponding signal-to-noise ratio (SNR) of the i th data stream on the k th subcarrier can be calculated by:

$$\gamma_i[k] = \left(\eta^2 \left| \sum_{n_r=1}^{N_r} \sum_{n_t=1}^{N_t} W_{i,n_r}[k] H_{n_r,n_t}[k] F_{n_t,i}[k] \right|^2 q_i[k] \right) \left(\sigma_{\text{clip}}^2 \sum_{n_r=1}^{N_r} \sum_{n_t=1}^{N_t} |W_{i,n_r}[k] H_{n_r,n_t}[k]|^2 + \eta^2 \sum_{\hat{i}=1, \hat{i} \neq i}^I \left| \sum_{n_r=1}^{N_r} \sum_{n_t=1}^{N_t} W_{i,n_r}[k] H_{n_r,n_t}[k] F_{n_t,\hat{i}}[k] \right|^2 q_{\hat{i}}[k] + \sum_{n_r=1}^I |W_{i,n_r}[k]|^2 \sigma_{\text{rx},n_r}^2 \right)^{-1}, \quad (11)$$

In this study, the well-known singular-value decomposition (SVD)-based precoding and post-detection are used, which remove inter-channel interference and convert MIMO channels to orthogonal parallel channels.

III. SPATIAL AND WAVELENGTH CHARACTERISTICS OF MIMO-OFDM CHANNEL

In this section, we introduce the characteristics of the MIMO-OFDM channel \mathbf{H}_k introduced in Section II. The relationship between the channel and parameters in the space, wavelength and frequency domains is considered. Firstly, we consider the discrete samples forwarded to the n_t th LED and its driving circuit. The discrete samples $\hat{x}_{n_t}[n]$ are converted to a continuous analogue signal via a pulse shaping process:

$$\tilde{x}_{n_t}(t) = \sum_{n=-\infty}^{\infty} \hat{x}_{n_t}[n] g(t - nT_s), \quad (12)$$

where $g(t)$ is the impulse response of the signal pulse and T_s is the symbol period. Before feeding the analogue signal, $\tilde{x}_{n_t}(t)$ is amplified by a factor of a_{n_t} and a direct current (DC)-bias of b_{n_t} is added in the driving circuit. The optical signal of the n_t th LED can be written as:

$$p_{n_t}(t, \lambda) = \mathcal{S}_{n_t}^{\text{led}}(\lambda) (a_{n_t} \tilde{x}_{n_t}(t) + b_{n_t}) \otimes h^{\text{led}}(t), \quad (13)$$

where $\mathcal{S}_{n_t}^{\text{led}}(\lambda)$ is the normalized spectral density of the n_t th LED at wavelength λ and $h^{\text{led}}(t)$ is the impulse response of the LED. After the emission of the optical signal to the wireless channel, a fraction of the signal is detected by the PDs on the receiver side. The output photocurrent of the n_r th PD can be written as:

$$i_{n_r}(t) = \int_{\lambda_{\min}}^{\lambda_{\max}} \mathcal{R}^{\text{pd}}(\lambda) h^{\text{pd}}(t) \otimes h_{n_r,n_t}^{\text{ow}}(t, \lambda) \otimes p_{n_t}(t, \lambda) d\lambda, \quad (14)$$

where $\mathcal{R}^{\text{pd}}(\lambda)$ is the spectral PD responsivity, $h^{\text{pd}}(t)$ is the low-pass impulse response of the PD and $h_{n_r,n_t}^{\text{ow}}(t, \lambda)$ is the optical wireless channel impulse response. Since the optical transmission

operates in a wide spectrum region, the final photocurrent is the result of an integration over the involved spectrum region. Then the photocurrent is forwarded to a matched filter, where the detected waveform is convolved with the signal pulse $g(t)$ and the discrete signal is obtained by sampling at nT_s . By applying a discrete-time unit impulse function input $\hat{x}_{n_t}[n] = \delta[n]$ to (12) and inserting (12), (13) into (14), the continuous channel impulse response before sampling can be calculated as:

$$h_{n_r, n_t}(t) = \int_{\lambda_{\min}}^{\lambda_{\max}} \mathcal{R}^{\text{pd}}(\lambda) \mathcal{S}_{n_t}^{\text{led}}(\lambda) g(t) \otimes h^{\text{pd}}(t) \otimes h_{n_r, n_t}^{\text{ow}}(t, \lambda) \otimes h^{\text{led}}(t) \otimes (a_{n_t} g(t) + b_{n_t}) d\lambda. \quad (15)$$

Noting that the convolution operation is with respect to t , but the integral is with respect to λ . The Fourier transform of (15) can be calculated as:

$$H_{n_r, n_t}(f) = \int_{\lambda_{\min}}^{\lambda_{\max}} \mathcal{R}^{\text{pd}}(\lambda) \mathcal{S}_{n_t}^{\text{led}}(\lambda) G(f) H^{\text{pd}}(f) H_{n_r, n_t}^{\text{ow}}(f, \lambda) H^{\text{led}}(f) (a_{n_t} G(f) + b_{n_t} \delta(f)) d\lambda, \quad (16)$$

where $G(f)$, $H^{\text{pd}}(f)$, $H_{n_r, n_t}^{\text{ow}}(f, \lambda)$ and $H^{\text{led}}(f)$ are the FFT of $g(t)$, $h^{\text{pd}}(t)$, $h_{n_r, n_t}^{\text{ow}}(t, \lambda)$ and $h^{\text{led}}(t)$, respectively. Based on the definition of discrete-time Fourier transform (DTFT), the channel transfer function after the matched filter sampling at nT_s is a periodic summation of $H_{n_r, n_t}(f)$ with a period of $1/T_s$ as: $H_{n_r, n_t}^{1/T_s}(f) = \sum_{l=-\infty}^{\infty} H_{n_r, n_t}(f - l/T_s)$. Thus the channel transfer function between the n_t th LED and the n_r th PD on the k th subcarrier can be calculated as:

$$H_{n_r, n_t}[k] = H_{n_r, n_t}^{1/T_s}\left(\frac{k}{KT_s}\right) = \sum_{l=-\infty}^{\infty} H_{n_r, n_t}\left(\frac{k}{KT_s} - \frac{l}{T_s}\right), \quad (17)$$

for $k = 0, 1, \dots, K - 1$. Although the limits of the summation in (17) are from $-\infty$ to ∞ , the band-limited signal pulse $G(f)$ makes most of the terms in the summation equal zero. For example, the used root-square raised cosine (RRC) pulse in this work makes the shifted channel frequency response (16) equals zero for $f \in \left(-\infty, -\frac{\alpha+1}{2T_s} + \frac{l}{T_s}\right) \cup \left(\frac{\alpha+1}{2T_s} + \frac{l}{T_s}, \infty\right)$. The subcarrier index of the transfer function falls in the region of $[0, K - 1]$, which is within the frequency range of $[0, 1/T_s)$. This implies that only the terms with $l = 0$ and 1 are non-zero in (17).

A. LED electrical-to-optical conversion

In (13), the choice of a_{n_t} and b_{n_t} should map the peak values of the input signal to the peak values of the optical output to maximise the signal power, as illustrated in Fig. 2a. Assuming the

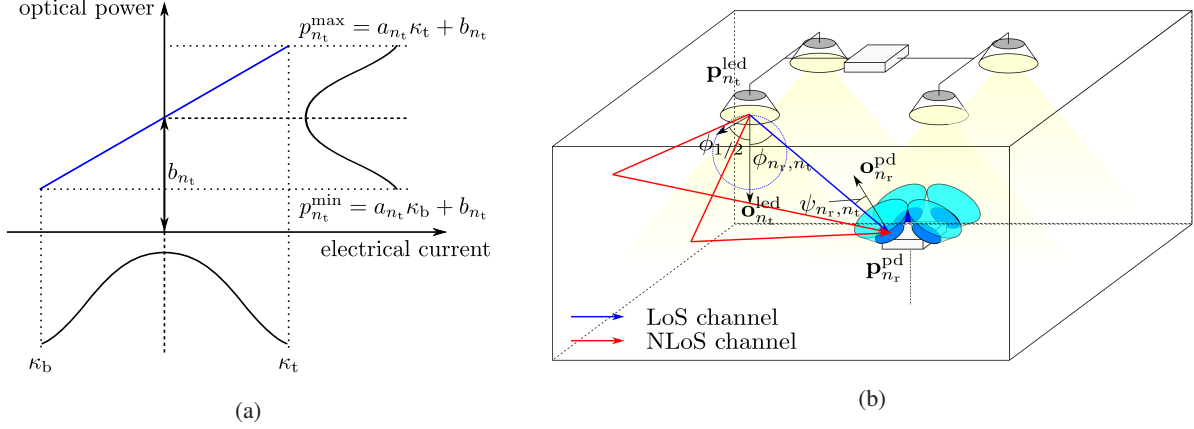


Figure 2: (a) Electrical to optical signal conversion. (b) Spatial-domain characteristics with LoS and NLoS channel components.

n_t th LED has a maximum and minimum optical levels of $p_{n_t}^{\max}$ and $p_{n_t}^{\min}$, the following mapping equations can be used: $a_{n_t}\kappa_b + b_{n_t} = p_{n_t}^{\min}$, $a_{n_t}\kappa_t + b_{n_t} = p_{n_t}^{\max}$, which lead to:

$$a_{n_t} = \frac{p_{n_t}^{\max} - p_{n_t}^{\min}}{\kappa_t - \kappa_b}, \quad b_{n_t} = \frac{p_{n_t}^{\min}\kappa_t - p_{n_t}^{\max}\kappa_b}{\kappa_t - \kappa_b}. \quad (18)$$

By using (13), the average optical power of the n_t th LED can be calculated by:

$$\bar{p}_{n_t} = \lim_{T \rightarrow \infty} \int_{-T}^T \int_{\lambda_{\min}}^{\lambda_{\max}} \frac{p_{n_t}(t, \lambda)}{2T} d\lambda dt = a_{n_t} \mathbb{E} \{ \hat{x}_{n_t}[n] \} + b_{n_t}, \quad (19)$$

where $\mathbb{E} \{ \hat{x}_{n_t}[n] \}$ is the expectation of the clipped signal, which can be evaluated analytically [29]. For simplicity of the analysis, we consider a symmetric clipping ($\kappa_t = \kappa$ and $\kappa_b = -\kappa$) and a zero minimum optical power level ($p_{n_t}^{\min} = 0$). This leads to simplification to (18) and (19) as $a_{n_t} = p_{n_t}^{\max}/2\kappa$, $b_{n_t} = p_{n_t}^{\max}/2 = \bar{p}_{n_t}$ and $\bar{p}_{n_t} = b_{n_t}$. If we consider \bar{p}_{n_t} as the given parameter, the scaling factor and DC-bias can be calculated by $a_{n_t} = \bar{p}_{n_t}/\kappa$ and \bar{p}_{n_t} .

B. Spatial-domain characteristics

The spatial-domain characteristics are primarily determined by the optical wireless channel between the LEDs and the PDs, which can be decomposed into a line-of-sight (LoS) component and non-line-of-sight (NLoS) components, as shown in Fig. 2b. The corresponding transfer function can be defined as: $H_{n_r, n_t}^{\text{ow}}(f, \lambda) = H_{n_r, n_t}^{\text{LoS}}(f, \lambda) + H_{n_r, n_t}^{\text{NLoS}}(f, \lambda)$. The LoS corresponds to the signal propagation directly from the LEDs to the PDs, which dominates the MIMO channel in most cases. The frequency response can be calculated as [30]:

$$H_{n_r, n_t}^{\text{LoS}}(f, \lambda) = \frac{(m_{\text{led}} + 1) A_{\text{pd}} \mathbf{1}_v}{2\pi D_{n_r, n_t}^2} \exp(-j2\pi f \tau_{n_r, n_t}) \mathcal{G}_{n_r}^{\text{of}}(\lambda, \psi_{n_r, n_t}) \cos^{m_{\text{led}}} \phi_{n_r, n_t} \cos^{m_{\text{fov}}} \psi_{n_r, n_t}, \quad (20)$$

where A_{pd} is the active area of the PD, m_{led} is the Lambertian emission order of the LED, m_{fov} is the field-of-view (FoV) coefficient [23], $\mathbf{1}_v$ is a visibility function, $\mathcal{G}_{n_r}^{\text{of}}(\lambda, \psi)$ is the transmittance of the optical filter mounted on the n_r th PD and D_{n_r, n_t} , ϕ_{n_r, n_t} , ψ_{n_r, n_t} , τ_{n_r, n_t} are the Euclidean distance, radiant angle, incident angle, time delay between the n_t th LED and the n_r th PD, respectively. The Lambertian emission order m_{led} is related to the LED half-power seminangle by $m_{\text{led}} = -1/\log_2(\cos(\phi_{1/2}))$. The time delay can be calculated by $\tau_{n_r, n_t} = D_{n_r, n_t}/c$, where $c = 3 \times 10^8$ m/s is the speed of light. The visibility function is defined as:

$$\mathbf{1}_v = \begin{cases} 1 & : \phi < \pi/2 \text{ and } \psi < \pi/2 \\ 0 & : \text{otherwise} \end{cases}, \quad (21)$$

which forces the channel to be zero when either ϕ or ψ exceed $\pi/2$. The value of (20) is directly determined by the positions and orientations of the LEDs and PDs. The trigonometric and distance terms in (20) can be calculated by [31]:

$$D_{n_r, n_t} = \|\mathbf{p}_{n_t}^{\text{led}} - \mathbf{p}_{n_r}^{\text{pd}}\|, \quad \cos \phi_{n_r, n_t} = \frac{\mathbf{o}_{n_t}^{\text{led}}}{D_{n_r, n_t}} \cdot (\mathbf{p}_{n_r}^{\text{pd}} - \mathbf{p}_{n_t}^{\text{led}}), \quad \cos \psi_{n_r, n_t} = \frac{\mathbf{o}_{n_r}^{\text{pd}}}{D_{n_r, n_t}} \cdot (\mathbf{p}_{n_t}^{\text{led}} - \mathbf{p}_{n_r}^{\text{pd}}), \quad (22)$$

where $\mathbf{p}_{n_t}^{\text{led}}$ and $\mathbf{o}_{n_t}^{\text{led}}$ are the position and orientation vectors of the n_t th LED, respectively; $\mathbf{p}_{n_r}^{\text{pd}}$ and $\mathbf{o}_{n_r}^{\text{pd}}$ are the position and orientation vectors of the n_r th PD, respectively; $\{\cdot\}$ refers to the vector dot product and $\|\cdot\|$ refers to the Euclidean norm. Note that the characteristics of $\mathcal{G}_{n_r}^{\text{of}}(\lambda, \psi)$ are affected by features in both the spatial and wavelength domains, which will be covered in Section III-C. [The NLoS channel responses correspond to the signal propagation via reflections by the room internal surfaces, which can be evaluated using an efficient frequency-domain simulation method \[30\].](#)

C. Wavelength-domain characteristics

Regarding the wavelength-domain characteristics, analytical spectrum models are used to improve the flexibility to configure the joint multiplexing system. The LED normalised spectral intensity can be defined by [13]:

$$\mathcal{S}_{n_t}^{\text{led}}(\lambda) = \frac{\frac{2}{\sqrt{\pi}} \exp\left(-\frac{(\lambda - \lambda_{n_t}^{\text{led},c})^2}{\Delta\lambda_{0.5}^2}\right) + \frac{4}{\sqrt{\pi}} \exp\left(-\frac{5(\lambda - \lambda_{n_t}^{\text{led},c})^2}{\Delta\lambda_{0.5}^2}\right)}{\Delta\lambda_{0.5} \left(\frac{2+\sqrt{5}}{\sqrt{5}} + \text{erf}\left(\frac{\lambda_{n_t}^{\text{led},c}}{\Delta\lambda_{0.5}}\right) + \frac{2}{\sqrt{5}} \text{erf}\left(\frac{\sqrt{5}\lambda_{n_t}^{\text{led},c}}{\Delta\lambda_{0.5}}\right)\right)}, \quad (23)$$

where $\lambda_{n_t}^{\text{led,c}}$ is the central wavelength of the n_t th LED and $\Delta\lambda_{0.5}$ is a parameter determining the spectrum shape of the LED, which is defined as:

$$\Delta\lambda_{0.5} = \begin{cases} \frac{5.5\mathcal{K}_B T_j}{\hbar c} \left(\lambda_{n_t}^{\text{led,c}}\right)^2 & : \lambda_{n_t}^{\text{led,c}} \leq 560 \text{ nm} \\ \frac{2.5\mathcal{K}_B T_j}{\hbar c} \left(\lambda_{n_t}^{\text{led,c}}\right)^2 & : \lambda_{n_t}^{\text{led,c}} > 560 \text{ nm} \end{cases}, \quad (24)$$

where $\mathcal{K}_B = 1.38 \times 10^{-23}$ J/K is the Boltzmann's constant, $T_j = 300$ K is the active layer temperature and $\hbar = 6.63 \times 10^{-34}$ J/Hz is Planck's constant. Note that $\int_{\lambda_{\min}}^{\lambda_{\max}} \mathcal{S}_{n_t}^{\text{led}}(\lambda) d\lambda = 1$. This model has been demonstrated to be accurate compared to the off-the-shelf LED devices [13]. The PD spectral responsivity can be defined by the following expression [32]:

$$\mathcal{R}^{\text{pd}}(\lambda) = \frac{\eta_q \mathfrak{q} \lambda}{\hbar c}, \quad (25)$$

where η_q is the quantum efficiency and $\mathfrak{q} = 1.6 \times 10^{-19}$ C is the electric charge. Considering a thin-film optical bandpass filter mounted on the n_r th PD with a central passband wavelength of $\lambda_{n_r}^{\text{of,c}}$ and a passband width of $\Delta\lambda^{\text{of}}$ at 0° incident angle, the spectral transmittance of the filter can be modelled by [26]:

$$\mathcal{G}_{n_r}^{\text{of}}(\lambda, \psi) = \begin{cases} \mathcal{G}_T & : \lambda_{n_r}^{\text{of,l}}(\psi) \leq \lambda \leq \lambda_{n_r}^{\text{of,r}}(\psi) \\ 0 & : \text{otherwise} \end{cases}, \quad (26)$$

where \mathcal{G}_T is the transmittance of the optical filter, $\lambda_{n_r}^{\text{of,l}}(\psi)$ and $\lambda_{n_r}^{\text{of,r}}(\psi)$ are left and right edges of the filter passband, which are functions of the incident angle ψ :

$$\lambda_{n_r}^{\text{of,l}}(\psi) = \left(\lambda_{n_r}^{\text{of,c}} - \Delta\lambda^{\text{of}}/2\right) \sqrt{1 - \sin^2 \psi / n_e^2}, \quad (27)$$

$$\lambda_{n_r}^{\text{of,r}}(\psi) = \left(\lambda_{n_r}^{\text{of,c}} + \Delta\lambda^{\text{of}}/2\right) \sqrt{1 - \sin^2 \psi / n_e^2}, \quad (28)$$

and n_e is defined as the effective refraction index. Several examples of (23), (25) and (26) have been depicted in Fig. 3a. It is worth noting that the passbands of the four plotted optical filters shift to shorter wavelengths significantly when the light incident angle changes from $\psi = 0^\circ$ to $\psi = 60^\circ$. In indoor VLC/LiFi applications, desired detector alignment is unlikely. Therefore, it is important to consider this bandpass shift characteristic.

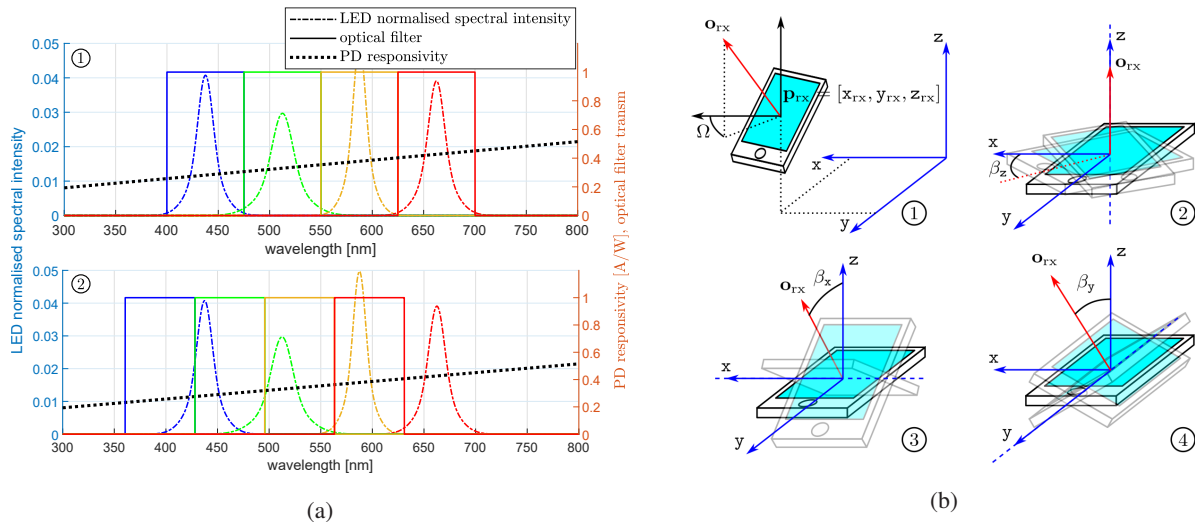


Figure 3: (a) Illustration of wavelength-dependent quantities. 1) incident angle $\psi = 0^\circ$ 2) incident angle $\psi = 60^\circ$. The central wavelength of the LED spectra and optical filter passbands at 0° incident angle are 437.5 nm, 512.5 nm, 587.5 nm and 662.5 nm. The optical filter passband width is 75 nm. (b) 1) UE position and horizontal orientation geometry. 2) UE rotation about z-axis. 3) UE rotation about x-axis. 4) UE rotation about y-axis.

D. Receiver noise model

Assuming that the background light power is negligible compared to the optical signal power, the dominant receiver noise components are the signal-dependent shot noise and the thermal noise. Therefore, the receiver noise variance can be calculated as:

$$\sigma_{r_x, n_r}^2 = 2q\tilde{i}_{n_r}B_s + \frac{4\mathcal{K}_B\mathcal{T}_aB_s}{R_L}, \quad (29)$$

where \tilde{i}_{n_r} is the photocurrent of the n_r th PD, $B_s = 1/2T_s$ is the signalling bandwidth and \mathcal{T}_a is the absolute temperature. For simplicity, the average photocurrent is used for the value of \tilde{i}_{n_r} .

IV. PERFORMANCE EVALUATION WITH VARIOUS SYSTEM CONFIGURATIONS

In Section III, it has been shown that the MIMO-OFDM channel is determined by many different parameters in the spatial and wavelength domains. In this section, we focus on exploring various system configurations. Specifically, we evaluate the performance of joint multiplexing systems with different sets of spatial and wavelength domain parameters, such as transmitter position $\mathbf{p}_{n_t}^{\text{led}}$ or optical filter passband $\Delta\lambda^{\text{of}}$. In a multiplexing system, the number of multiplexing channels has a significant impact on the aggregate data rate, which is determined by $\min(N_t, N_r)$. When evaluating the performance of joint multiplexing systems scaling with the number of LEDs/PDs, the data rate varies slightly if only one of the variables (number of LEDs or PDs)

is changed. To avoid generating trivial results that are less meaningful, the numbers of LEDs and PDs are always identical ($N_t = N_r = I$) in the considered MIMO-OFDM systems in the following sections. For the convenience of description, we define a variable called the ‘number of elements’ which is equivalent to the number of LEDs, PDs and data streams. In addition, to reduce the complexity of the metric evaluation, a uniform power allocation is used in this section: $q_i[k] = K/(K - 2)$.

A. Performance metric: average achievable rate with random user equipment (UE) position and orientation

Firstly, we define the average achievable rate as the performance metric. Since the calculated SNR in (11) corresponds to complex bipolar QAM symbols after a series of conversions, the achievable rate can be evaluated by [33]:

$$C = \frac{1}{T_s (K + N_{cp})} \sum_{i=1}^I \sum_{k=1}^{\tilde{K}} \log_2 \left(1 + \frac{\gamma_i[k]}{\Gamma} \right), \quad (30)$$

where $\gamma_i[k]$ is the SNR and Γ is a gap factor between the achievable rate and the Shannon capacity, which is empirically configured to compensate the system impairment and imperfect constellation [33]. Most of the parameters related to the SNR calculation are determined by the system configuration only, such as spectrum intensity or radiation pattern of an LED. However, the position and orientation of PDs are determined by the user behaviour. Therefore, the randomness in UE position and orientation is considered in the evaluation of the achievable rate.

The UE geometry is depicted in Fig. 3b 1). The three-dimensional (3D) position vector of the UE is defined as $\mathbf{p}_{rx} = [x_{rx}, y_{rx}, z_{rx}]$, where the x_{rx} and y_{rx} are the two-dimensional (2D) coordinate of the UE and z_{rx} is the UE height from the floor level, which is assumed to be deterministic in this study. It is also assumed that the size of the receiver is small, relative to the link distance, so that the multiple PDs mounted on the receiver are collocated. Thus, the position vector of the n_r -th PD is the same as the UE position: $\mathbf{p}_{n_r}^{pd} = \mathbf{p}_{rx}$. In addition, an azimuth angle Ω is defined to determine the horizontal direction of the UE. Since there is no bias on the user position and the azimuth angle, it is assumed that these quantities are uniformly distributed, which have been widely accepted in the wireless communication research community: $x_{rx} \sim \mathcal{U}_{(0, W_{room})}$, $y_{rx} \sim \mathcal{U}_{(0, L_{room})}$ and $\Omega \sim \mathcal{U}_{(0, 2\pi]}$, where \mathcal{U}_I refers to the continuous uniform distribution with an interval I . The notations L_{room} and W_{room} correspond to the length and width of the room.

Table I: Upward and random orientations rotation angle characteristics

	(a) upward	(b) random	
	value	mean μ	standard deviation $\sqrt{2}b$
β_z	$\Omega - 90^\circ$	$\Omega - 90^\circ$	3.67°
β_x	0°	40.78°	2.39°
β_y	0°	-0.84°	2.21°

In addition to the random user position and horizontal direction, two user device orientation scenarios are considered in this study. The random orientation of the UE is defined by three rotation angles: β_z , β_x and β_y which correspond to the yaw, pitch and roll rotations about the z, x and y-axes, as illustrated in Fig. 3b 2), 3) and 4). Then, the PD orientation vector $\mathbf{o}_{n_r}^{\text{pd}}$ is determined by:

$$\left[\mathbf{o}_{n_r}^{\text{pd}}\right]^T = \mathbf{R}_z \mathbf{R}_x \mathbf{R}_y \left[\mathbf{o}_{n_r}^{\text{pd},\uparrow}\right]^T, \quad (31)$$

where $\mathbf{o}_{n_r}^{\text{pd},\uparrow}$ is the PD orientation vector of the n_r th PD when the UE has an upward facing orientation with the normal vector of $\mathbf{o}_{\text{rx}} = [0, 0, 1]$; \mathbf{R}_z , \mathbf{R}_x and \mathbf{R}_y are 3D rotation matrices corresponding to β_z , β_x and β_y , respectively. They are defined by:

$$\mathbf{R}_z = \begin{bmatrix} \cos \beta_z & -\sin \beta_z & 0 \\ \sin \beta_z & \cos \beta_z & 0 \\ 0 & 0 & 1 \end{bmatrix}, \quad \mathbf{R}_x = \begin{bmatrix} 1 & 0 & 0 \\ 0 & \cos \beta_x & -\sin \beta_x \\ 0 & \sin \beta_x & \cos \beta_x \end{bmatrix}, \quad \mathbf{R}_y = \begin{bmatrix} \cos \beta_y & 0 & \sin \beta_y \\ 0 & 1 & 0 \\ -\sin \beta_y & 0 & \cos \beta_y \end{bmatrix}. \quad (32)$$

In the first scenario, an upward facing UE is considered, which corresponds to large devices such as laptops. In this case, we have $\beta_z = \Omega - 90^\circ$ and $\beta_x = \beta_y = 0^\circ$, as concluded in Table I (a). In the second scenario, hand-held devices are considered with a random orientation. The statistics of β_z , β_x and β_y have been obtained via experimental measurement and modelled using Laplace and Gaussian distributions [34]. For sitting users, the three rotation angles follow Laplace distributions: $\beta \sim \mathcal{L}(\mu, b)$ with a mean value of μ and a standard deviation of $\sqrt{2}b$. The means and standard deviations of different rotation angles are concluded in Table I (b). By incorporating the UE randomness, the average achievable rate can be evaluated by:

$$\bar{C} = \mathbb{E}_{x_{\text{rx}}, y_{\text{rx}}, \Omega} [C], \quad \bar{C} = \mathbb{E}_{x_{\text{rx}}, y_{\text{rx}}, \Omega, \beta_z, \beta_x, \beta_y} [C], \quad (33)$$

for the cases of upward and random orientation scenarios, respectively. Due to the complexity issues, these metrics have to be evaluated using a Monte Carlo approach.

B. System configuration with BADS algorithm

In this paper, the average achievable rates (33) with several sets of empirically selected parameters are evaluated. In addition, we aim to evaluate the maximum potential of the proposed joint multiplexing system in terms of achievable rate. With the number of parameters exceeding ten, it is very time-consuming to find the best system configuration parameters with an exhaustive search approach by testing all combinations of different parameter values. Therefore, a suitable optimisation tool is used to efficiently search the desired system configuration.

The optimisation objective function (33) is a complex function of the considered system parameters by equations from (11) to (30). Additionally, the numerical evaluation of (33) requires averaging over random user orientations and positions with a Monte-Carlo approach. This leads to a noisy, high dimensional and high complexity objective function, which cannot be solved by a conventional gradient-based optimisation method, such as linear programming. Instead, a state-of-the-art black-box optimisation tool is used to tackle this problem. Black-box optimisation methods are used when the objective function is unknown, non-smooth or complicated to evaluate, where the derivate of the objective function is unavailable, unreliable or impractical to calculate [35]. The used optimisation is known as BADS which combines the capability of Bayesian optimisation in optimising expensive and noisy black-box functions with the low computational cost of mesh adaptive direct search (MADS). It has been demonstrated that the BADS algorithm outperforms a number of widely used and state-of-the-art non-convex, derivative-free optimisation algorithms on many practical problems [36]. This type of optimisation methods have wide applications in the fields of computational neuroscience and machine learning where models are evaluated via stochastic simulation or numerical approximation [37].

The major operations in the BADS algorithm are introduced in Algorithm 1. The BADS algorithm considers a possibly noisy objective function $f(\mathbf{x})$ with an N_d dimension input variable vector $\mathbf{x} \in \mathbb{R}^{N_d}$. A lower bound vector \mathbf{x}_{LB} and an upper bound vector \mathbf{x}_{UB} must be provided as the constraints to the variable vector \mathbf{x} . An optional plausible bound vectors \mathbf{x}_{PLB} and \mathbf{x}_{PUB} can also be provided to indicate the regions where the optimal solutions are more likely. At the beginning of the algorithm, an initial solution \mathbf{x}_0 will be provided as a starting point. Then, the algorithm enters the search stage and executes a series of efficient local Bayesian optimisations around the point and try to find a solution which is better than the current one. Each new evaluation of the cost function is used as a new sample of the data set to re-train a Gaussian process model to be

Algorithm 1: Bayesian Adaptive Direct Search [36]

Initialise: $n_{\text{iter}} = 0$, $\Delta_0^m = 2^{-10}$, $\Delta_0^p = 1$, evaluate $f(\mathbf{x}_0)$

while $n_{\text{iter}} \leq N_{\text{iter,max}}$ *and* $\Delta_0^p > \Delta_{\text{th}}^p$ **do**

repeat

 | generate search input $\mathbf{x}_{\text{search}}$ and evaluate $f(\mathbf{x}_{\text{search}})$

until $f(\mathbf{x}_{\text{search}})$ *provides sufficient improvement or reaches maximum search number* N_{search} ;

if *Search stage is unsuccessful* **then**

 | generate poll set $P_{n_{\text{iter}}}$, sort it using the acquisition function and evaluate $f(\mathbf{x})$ on $\mathbf{x} \in P_{n_{\text{iter}}}$

end

if n_{iter} *th iteration is successful* **then**

 | update incumbent $\mathbf{x}_{n_{\text{iter}}+1}$

if *Poll stage is successful* **then**

 | $\Delta_{n_{\text{iter}}+1}^m = 2\Delta_{n_{\text{iter}}}^m$, $\Delta_{n_{\text{iter}}+1}^p = 2\Delta_{n_{\text{iter}}}^p$

end

else

 | $\Delta_{n_{\text{iter}}+1}^m = \frac{1}{2}\Delta_{n_{\text{iter}}}^m$, $\Delta_{n_{\text{iter}}+1}^p = \frac{1}{2}\Delta_{n_{\text{iter}}}^p$

end

$n_{\text{iter}} = n_{\text{iter}} + 1$

end

a more accurate surrogate. If the algorithm fails to find a better solution in the search stage, it means the current Gaussian process model is not useful in the optimisation. Then, the algorithm can switch to the poll stage which uses model-free opportunistic optimisation to compensate. The notations $\Delta_{n_{\text{iter}}}^m$ and $\Delta_{n_{\text{iter}}}^p$ are the mesh and poll size of the n_{iter} th iteration. They function as the adaption step sizes, which vary in the optimisation process. In unsuccessful iterations, $\Delta_{n_{\text{iter}}}^m$ and $\Delta_{n_{\text{iter}}}^p$ are decreased to increase the searching granularity. In successful iteration in the poll stage, they are increased to speed up the convergence speed. Finally, the algorithm ends when the poll size is smaller than a predefined threshold or the maximum number of iterations is reached.

More details about the implementation, convergence analysis, optimality condition and complexity of BADS can be found in [36], [38]. In this study, we have used the BADS algorithm implementation in MATLAB provided by the authors of [36]. It is worth noting that the BADS algorithm is a semi-local algorithm which may generate a global or a local optimal solution. To increase the chance of obtaining global optimal solutions, a multi-start strategy is used and the number of iterations with different initial solutions for each optimisation problem equals or greater than ten. In this study, the running time of executing the BADS algorithm with multiple iterations varies from a few seconds to tens of minutes with the increase of element number I .

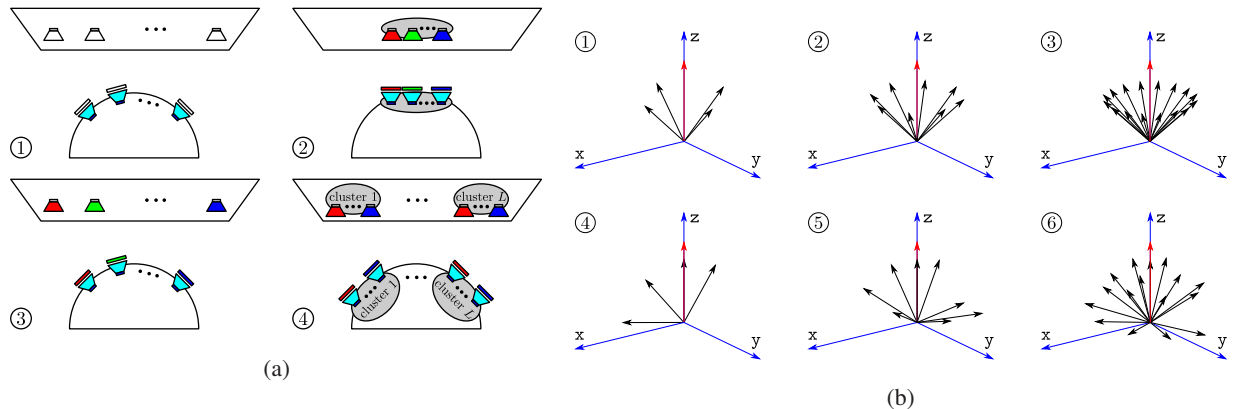


Figure 4: (a) Illustration of various LED layouts on the ceiling and PD orientations on the mobile side with different configuration strategies: 1) Division in space domain. 2) Division in wavelength domain. 3) Division in both spatial and wavelength domains. 4) Division in either spatial or wavelength domain. (b) Angular diversity receivers: 1), 2) and 3) show three PR examples with $N_r = 4, 8, 16$. 4), 5) and 6) show three HR examples with $N_r = 4, 8, 16$.

However, the obtained system configuration parameters from searching the problems with the BADS algorithm are static and used to implement the VLC joint multiplexing system. These obtained parameters are fixed once the system is implemented and will not change during the operation of the system. Therefore, unlike many signal processing algorithms, there is little computational complexity concerns about the use of BADS algorithm in this work.

C. Overview of system configuration strategies

Now we consider four potential configuration strategies: 1) division in the space domain, 2) division in the wavelength domain, 3) division in both the spatial and wavelength domains, 4) division in either the spatial or wavelength domain, as demonstrated in Fig. 4a. The first two strategies use the DoFs in the spatial or wavelength domain only, which are equivalent to SMX and WDM transmission systems, respectively. These two strategies are referred as space division (SD) and wavelength division (WD). They will be covered in Section IV-D and IV-E, respectively. The third and fourth strategies use the DoFs in the spatial and/or wavelength domain jointly. The third strategy considers each optical element has a distinct spatial and wavelength domain feature, as illustrated in Fig. 4a 3). This strategy leads to excessive decorrelation of the channel matrix at the cost of inefficient use of spatial and wavelength DoFs. In contrast, the fourth strategy considers to let each optical element to have a unique feature in either the spatial or wavelength domain, as illustrated in Fig. 4a 4). It is expected to provide enough channel matrix

decorrelation and also be able to support a greater number of multiplexing channels compared to the SD and WD strategies. This joint strategy will be covered in Section IV-F.

D. Spatial division strategy

Firstly, the configurable parameters considered in SD strategy is introduced. Since only the DoF in spatial domain is utilised for multiplexing transmission, wavelength domain parameters are empirically selected with identical values for all LEDs and optical filters: $\Delta\lambda^{\text{of}} = 300$ nm, $\lambda_{n_t}^{\text{led,c}} = 550$ nm for $n_t = 1, 2, \dots, N_t$ and $\lambda_{n_r}^{\text{of,c}} = 550$ nm for $n_r = 1, 2, \dots, N_r$. On the transmitter side, the position vector of the n_t th LED is defined as:

$$\mathbf{p}_{n_t}^{\text{led}} = [x_{n_t}, y_{n_t}, z_{\text{tx}}], \quad (34)$$

where z_{tx} is the height coordinate of the LEDs determined by the height of the room; x_{n_t} and y_{n_t} are the 2D horizontal coordinates of the LED, which are configurable parameters. Regarding the orientation of LEDs, a straight downward orientation of $\mathbf{o}_{n_t}^{\text{led}} = [0, 0, -1]$ is used to guarantee the lighting performance and a wide coverage. Finally, the radiation pattern is defined by the LED half-power semiangle $\phi_{1/2}$, which is another important configurable parameter. On the receiver side, it is impractical to control the exact position and orientation of each PD due to the random user location and orientation, while the FoV coefficient m_{fov} can be manipulated to control the light reception pattern, which is a configurable parameter of interest. On the other hand, the small UE size assumption prevents the effective spatial decorrelation using different PD positions. In order to achieve low spatial correlation on the receiver side, two types of angular diversity receivers are considered in this study: pyramid receiver (PR) and hemispheric receiver (HR) [23]. In equation (31), the upward facing PD orientation vector can be represented by $\mathbf{o}_{n_r}^{\text{pd},\uparrow} = [\cos \omega_{n_r} \sin \theta_{n_r}, \sin \omega_{n_r} \sin \theta_{n_r}, \cos \theta_{n_r}]$, where ω_{n_r} is a PD azimuth angle and θ_{n_r} is a PD elevation angle. In a PR, the values of θ_{n_r} is defined by a PR elevation angle θ_{pd} , which is a suitable configurable parameter. The PD azimuth angles are specified as:

$$\omega_{n_r} = \frac{2\pi}{N_r}(n_r - 1). \quad (35)$$

In a HR, the elevation angles are specified as:

$$\theta_{n_r} = \arccos(s_{n_r}), \quad (36)$$

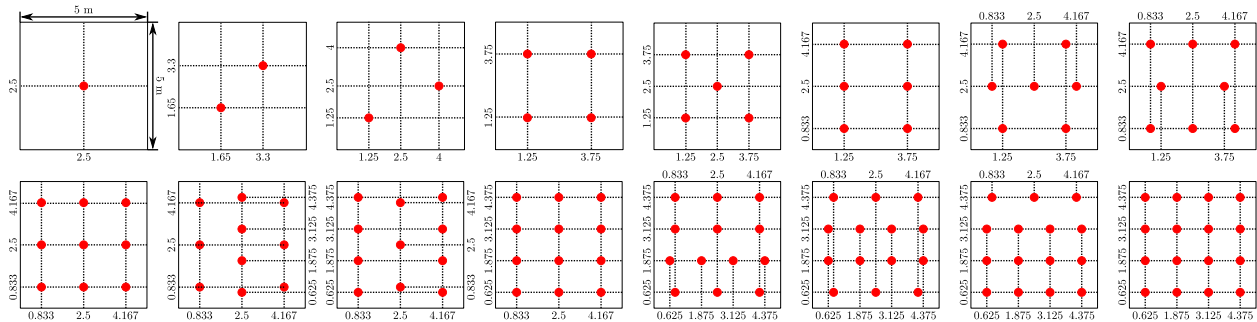


Figure 5: Empirical configuration to 2D LED position layout.

with $s_{n_r} = 1 - \frac{2(n_r-1)}{2N_r-1}$, and the azimuth angles are specified as:

$$\omega_{n_r} = \left(\omega_{n_r-1} + 3.6 \left(2N_r \left(1 - s_{n_r}^2 \right) \right)^{-1/2} \right) \text{mod } 2\pi, \quad (37)$$

for $n_r = 2, \dots, N_r$ and $\omega_1 = 0$. Fig. 4b demonstrate six examples of PRs and HRs with $N_r = 4, 8, 16$. In summary, the considered configurable parameters in the SD strategy include: x_{n_t} , y_{n_t} , $\phi_{1/2}$, m_{fov} , (θ_{pd}) . Note that θ_{pd} is only considered when PRs are used.

1) *Empirical configuration*: In cases with the empirical configuration, the values of x_{n_t} and y_{n_t} with different number of N_t are specified according to the 2D layouts shown in Fig. 5. The intuition of this LED spatial distribution is to distribute the LEDs with wider separations to guarantee a low spatial correlation on the transmitter side. On the other hand, the LEDs are distributed in a manner to let the system cover the entire room. An LED halfpower semiangle of $\phi_{1/2} = 60^\circ$ is used to ensure a wide coverage of each LED. An FoV coefficient of $m_{\text{fov}} = 1.4738$ is used as this value has been found to achieve a good match to practical PD characteristics [23]. In the case of PR, a PD elevation angle of $\theta_{\text{pd}} = 40^\circ$ is used as it has been demonstrated to achieve a high data rate in a MIMO system [23].

2) *Configuration with BADS algorithm*: It is straightforward to use the BADS algorithm introduced in Section IV-B to search system configuration parameters of interest with the following procedures: 1. Formulate a general black-box optimisation problem with the considered configurable parameters as input variables \mathbf{x} and average achievable data rate \bar{C} as the objective function. 2. Define bound vectors based on the practical constraints of the considered input variables. 3. Generate an initial solution vector \mathbf{x}_0 , where each variable is randomly selected from the values between the plausible bounds with equal probability. 4. Execute the BADS algorithm multiple times with different initial solutions. The black-box optimisation problem for

Table II

Parameters	Symbol	Values	Parameters	Symbol	Values
Room width/length/height [m]	$W_{\text{room}}/L_{\text{room}}/H_{\text{room}}$	5/5/3	DCO-OFDM clipping level	κ	3.2
Total optical power [W]	$\sum_{n_t=1}^{N_t} p_{n_t}$	80	PD physical area [cm ²]	A_{pd}	1
Height of LED/PD [m]	$z_{\text{tx}}/z_{\text{rx}}$	3/0.75	Number of subcarriers	K	256
Wavelength range [nm]	$\lambda_{\text{min}}/\lambda_{\text{max}}$	400/700	Modulation bandwidth [MHz]	$1/2T_s$	50
Optical filter transmittance	\mathcal{G}_T	1	LED/PD 3dB bandwidth [MHz]	$f_{\text{led,c}}$	35/106
PD quantum efficiency	η_q	0.8	Modulation gap factor	Γ	6.06 dB
Effective index	n_e	2	Cyclic-prefix	N_{cp}	30

system configurations with the SD strategy is defined as:

$$\underset{\mathcal{X}}{\text{maximise}} \quad \bar{C}^{\text{SD}}(\mathcal{X}) \text{ with } \mathcal{X} = \{x_{n_t}, y_{n_t}, \phi_{1/2}, m_{\text{fov}}, (\theta_{\text{pd}})\} \quad (38)$$

$$\text{subject to} \quad 0 < \frac{x_{n_t}}{W_{\text{room}}} < 1 \text{ for } n_t = 1, \dots, I, \quad (39)$$

$$0 < \frac{y_{n_t}}{L_{\text{room}}} < 1 \text{ for } n_t = 1, \dots, I, \quad (40)$$

$$0^\circ < \phi_{1/2} \leq 60^\circ, \quad (41)$$

$$m_{\text{fov}} \geq 1, \quad (42)$$

$$(0^\circ \leq \theta_{\text{pd}} \leq 90^\circ). \quad (43)$$

Note that θ_{pd} only exist in the optimisation with PR.

Fig. 6a shows the average achievable rate results against the number of elements (up to 16) achieved by systems with SD strategy. The remaining system parameters (irrelevant to DoF in the spatial domain) are listed in Table II. Regarding the gap factor value, it has been shown in [39] that a gap factor of 6 dB is sufficient for M -QAM modulation to achieve a bit error rate (BER) at 1×10^{-3} for $M = 2$. With an increase in M , the required gap factor decreases. This implies that by using a fixed gap factor of 6 dB is sufficient for the calculated achievable rate with a BER of 1×10^{-3} . Note that as the number of elements changes, the total transmission optical power stays the same and is equally distributed to each LED. Both cases with a PR and HR are presented. In addition, the cases with upward facing/random orientation scenarios and with empirical/optimised configurations are demonstrated. With an increase in the number of elements, the average achievable rate also increases due to more available multiplexing channels. However, a further increase in the number of elements (beyond 5 to 7) leads to a less average

achievable rate improvement, especially for the cases with empirical configurations using PR. This is because with a greater number of elements, the channel spatial correlation also increases. This leads to a channel matrix with worse channel conditions, which achieves fewer and weaker multiplexing channels. Intuitively, the performance of systems with optimised configurations are better than those with empirical configurations. With 16 elements, the average achievable rates by empirically configured systems are lower than 1100 Mbps, while the systems with optimised configurations achieved a sum rate in the range of 1100 to 1500 Mbps. On the other hand, systems with random orientation scenarios received a performance penalty compared to cases with upward facing receivers due to the more severe misalignment. Regarding different types of angular diversity receivers, the PRs offer better performance with a fewer number of elements, while the HR offers a slightly better performance with a large numbers of elements.

E. Wavelength division strategy

In cases employing the WD strategy, the joint multiplexing system is equivalent to a conventional WDM system with MIMO processing techniques, which is similar to those in [14]. All spatial domain parameters are empirically defined as follows: all LEDs are located in the centre of the room $\mathbf{p}_{n_t}^{\text{led}} = [W_{\text{room}}/2, L_{\text{room}}/2, z_{\text{tx}}]$ with an orientation of $\mathbf{o}_{n_t}^{\text{led}} = [0, 0, -1]$ and all PDs have the same orientation of $\mathbf{o}_{n_r}^{\text{pd}, \uparrow} = [0, 0, 1]$. The wavelength domain configurable parameters of interest in cases with the WD strategy include the LED central wavelength $\lambda_{n_t}^{\text{led}, c}$, optical filter passband centre $\lambda_{n_r}^{\text{of}, c}$ and optical filter passband width $\Delta\lambda^{\text{of}}$.

1) *With and without MIMO processing:* With the WD strategy, the precoding and post-detection process transform the ‘colour’-MIMO channel matrix with inter-colour crosstalk to a diagonal matrix. This operation is expected to mitigate the excessive crosstalk caused by the bandpass shift phenomenon. To highlight this important feature, the results of conventional WDM systems without MIMO processing are also included for comparison. In the case of conventional WDM systems, the precoding and post-detection matrices are set to identity matrices: $\mathbf{F}_k = \mathbf{W}_k = \mathbf{I}$, where \mathbf{I} is defined as an identity matrix.

2) *Empirical configuration:* In the case of empirical configurations, the passband width of optical filters are defined by:

$$\Delta\lambda^{\text{of}} = (\lambda_{\text{max}} - \lambda_{\text{min}})/I. \quad (44)$$

The intuition of this setting is that the passband should be wide enough to accept most of the signal power from one LED, but not too wide to receive too much power from LEDs of other

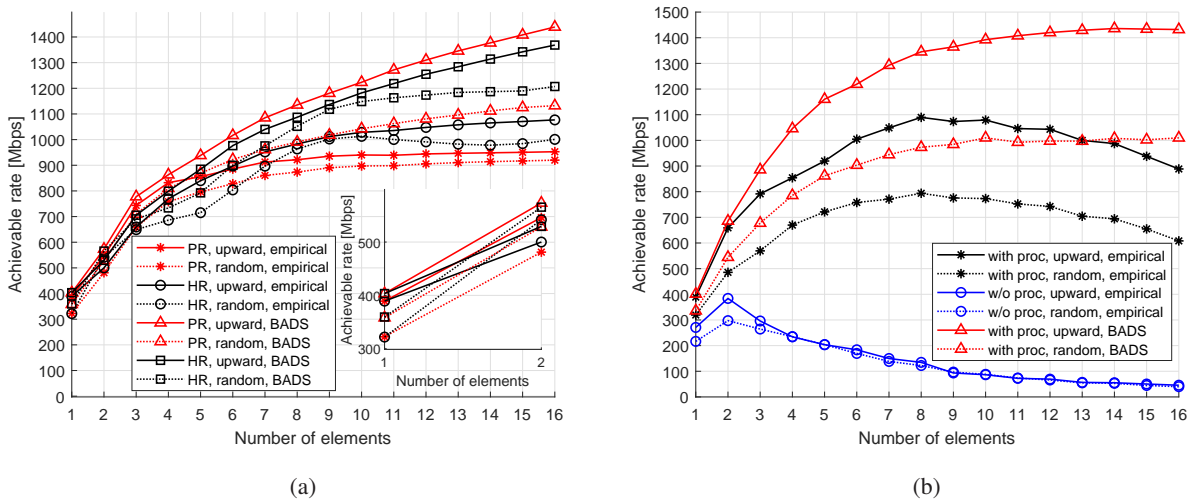


Figure 6: Average achievable rate against number of elements achieved by joint multiplexing systems with (a) SD strategy and (b) WD strategy. 'upward' and 'random' refer to the upward facing receiver scenario and random orientation scenario, respectively. 'with proc' and 'w/o proc' refer to with MIMO processing and without MIMO processing, respectively.

colours. In addition, the spectrum centre of the i th LED and the passband centre of the i th optical filter are defined by:

$$\lambda_i^{\text{led},c} = \lambda_i^{\text{of},c} = \lambda_{\min} + (i - 0.5)\Delta\lambda^{\text{of}}. \quad (45)$$

These configurations aim to uniformly distribute the spectra of LEDs and the passband of optical filters within the visible light spectrum.

3) *Configuration with BADS algorithm*: The parameter searching using the BADS algorithm with WD strategy is similar to that in Section IV-D2 except that the black-box optimisation problem is redefined as follows:

$$\underset{\mathcal{X}}{\text{maximise}} \quad \bar{C}^{\text{WD}}(\mathcal{X}) \text{ with } \mathcal{X} = \{\lambda_{n_t}^{\text{led},c}, \lambda_{n_r}^{\text{of},c}, \Delta\lambda^{\text{of}}\} \quad (46)$$

$$\text{subject to} \quad \lambda_{\min} \leq \lambda_{n_t}^{\text{led},c} \leq \lambda_{\max} \text{ for } n_t = 1, \dots, I, \quad (47)$$

$$\lambda_{\min} \leq \lambda_{n_r}^{\text{of},c} \leq \lambda_{\max} \text{ for } n_r = 1, \dots, I, \quad (48)$$

$$\Delta\lambda^{\text{of}} > 0. \quad (49)$$

Fig. 6b shows the average achievable rates achieved by joint multiplexing systems with WD strategy against the number of elements. The remaining system parameters are the same as those listed in Table II. It can be observed that the highest average achievable rate by the systems without MIMO processing is less than 400 Mbps at two elements. This demonstrates

the severe performance penalty caused by the bandpass shift issue and the excessive inter-colour interference with a large number of WDs. Therefore, the MIMO processing is important for joint multiplexing systems with WD strategy. In contrast, the average rates achieved by systems with MIMO processing increase with the number of elements consistently when the number of elements is small. However, when the number of elements is between 7 to 9, a further increase in the number of elements no longer provides an effective boost to the average achievable rate. In actuality, the achievable rates drop with an increase of the number of elements in the cases of empirical configurations. In the cases of configuration with a BADS algorithm, the performance degradation with an optical element increase can be avoided, but no further improvement can be observed either, as shown in Fig. 6b. This is because the use of optical filters with a narrow passband actively block a significant amount of optical power from LEDs. The narrower the optical filter passband, the more power loss occurs, which leads to a more severe degradation in the overall SNRs and achievable rate. In addition, the increased number of elements leads to a more severe spectrum overlap between adjacent WD channels, which causes significant correlations between WD channels. Consequently, the multiplexing channels with smaller eigenvalues are severely degraded. Compared to cases with SD strategy, all LEDs and PDs have the same orientation and positions. When there is a good alignment, all multiplexing channels are achieving high SNR and capacity. When there is a bad alignment, none of the channels show a good performance. The issue is more severe in the case of random orientation scenarios. This situation is quite different from the SD systems where the chance of at least one or a few good channels is much higher due to the better spatial diversity. Note that the performance gap between upward scenario and corresponding random orientation scenario is smaller in SD systems.

F. Spatial clustering with wavelength division strategy

In Section IV-D and IV-E, the limitation of SD and WD strategies has been demonstrated. In this section, the configurations based on the approach of ‘division in either the space or wavelength domain’ are considered. The proposed strategy is named as SCWD. The basic idea of the SCWD scenario is to divide the LEDs and PDs into multiple groups. The optical elements in each group are clustered with the same positions and orientations, as illustrated in Fig. 4a (d). Thus, the optical elements in different groups/clusters have different spatial features to decorrelate the channel. On the other hand, LEDs in the same cluster have different spectra, and optical

Algorithm 2: Cluster-to-element variable mapping

```

Initialise cluster index:  $l = 1$ 
for  $i = 1, 2, \dots, I$  do
   $M_{\text{sum}} = \sum_{\hat{i}=1}^l M_{\hat{i}}$ 
  if  $i > M_{\text{sum}}$  then
    Cluster index increment:  $l = l + 1$ 
  end
   $m = i - M_{\text{sum}} + M_l$ 
  Variable mapping:  $x_i = x_l, y_i = y_l, \omega_i = \omega_l, \theta_i = \theta_l, \lambda_i^{\text{led}} = \lambda_{c,m}^{\text{led}}, \lambda_i^{\text{of}} = \lambda_{c,m}^{\text{of}}$ 
end

```

filters with different passbands are mounted on PDs in the same cluster. This wavelength division can remove the channel correlation between optical elements within the same group/cluster.

Next, the details about the proposed SCWD strategy will be introduced. Assume that the MIMO-OFDM system has I LEDs and PDs divided into L clusters, where $1 \leq L \leq I$. The configuration of spatial variables is similar to that introduced in Section IV-D except that the configuration is with respect to each spatial cluster instead of each individual optical element. On the transmitter side, the l th LED cluster has a position of:

$$\mathbf{p}_{c,l}^{\text{led}} = [x_l, y_l, z_{\text{tx}}], \quad (50)$$

for $l = 1, 2, \dots, L$, where x_l and y_l are the horizontal coordinates of the l th LED cluster, which are configurable parameters. All LED clusters have the same orientation of $[0, 0, -1]$. In the case of an upward facing receiver, the l th PD cluster has an orientation vector of:

$$\mathbf{o}_{c,l}^{\text{pd},\uparrow} = [\cos \omega_l \sin \theta_l, \sin \omega_l \sin \theta_l, \cos \theta_l], \quad (51)$$

where ω_l and θ_l are the azimuth angle and elevation angle of the l th PD cluster, which are defined based on the characteristics of PR and HR using (35), (36) and (37). Similar to the SD strategy, $\phi_{1/2}$, \mathbf{m}_{fov} and (θ_{pd}) are also spatial domain configurable parameters. The number of optical elements in the l th cluster is defined as:

$$M_l = \begin{cases} \lceil I/L \rceil & : l \leq \text{mod}(I, L) \\ \lfloor I/L \rfloor & : \text{otherwise} \end{cases}, \quad (52)$$

which ensure the sizes of different clusters are similar to a maximum difference of one element. Note that $\lceil \cdot \rceil$ and $\lfloor \cdot \rfloor$ are defined as the ceiling and floor operators, respectively. This also implies that the maximum required number of WD is $\lceil I/L \rceil$. Within the l th cluster, the central wavelength

of the m th LED is defined as $\lambda_{c,m}^{\text{led}}$ on the transmitter side for $m = 1, 2, \dots, M_l$. On the receiver side, the passband centre of the m th optical filter is defined as $\lambda_{c,m}^{\text{of}}$. Opposite to the spatial parameter configurations, the wavelength domain parameters are identical in different clusters. Similar to the WD strategy, in addition to $\lambda_{c,m}^{\text{led}}$ and $\lambda_{c,m}^{\text{of}}$, the optical filter passband with $\Delta\lambda^{\text{of}}$ is also a configurable parameter. By unifying some of the parameters, the system configuration process can be significantly simplified. If the configuration is with respect to each element, the number of configurable parameters will be $4I+4$. With the cluster-based configuration, there are $2(L + \lceil I/L \rceil) + 4$ configurable parameters, which include: $x_l, y_l, \lambda_{c,m}^{\text{led}}, \lambda_{c,m}^{\text{of}}, \phi_{1/2}, \mathbf{m}_{\text{fov}}, (\theta_{\text{pd}}), \Delta\lambda^{\text{of}}$.

With cluster-based parameters $x_l, y_l, \omega_l, \theta_l, \lambda_{c,m}^{\text{led}}, \lambda_{c,m}^{\text{of}}$, the corresponding parameters with respect to the i th optical element $x_i, y_i, \omega_i, \theta_i, \lambda_i^{\text{led}}, \lambda_i^{\text{of}}$ can be obtained using Algorithm 2. With a given set of spatial and wavelength domain parameters, the average achievable rate with a specific number of clusters L can be calculated. However, it is not straightforward to select L that achieves the highest average achievable rate. Therefore, the average achievable rates with all possible numbers of clusters \bar{C}_L^{SCWD} are evaluated for $L = 1, 2, \dots, I$. Finally, we find the result achieves the highest average achievable rate among the evaluations with different L as:

$$\bar{C}^{\text{SCWD}} = \max \{ \bar{C}_{L=1}^{\text{SCWD}}, \bar{C}_{L=2}^{\text{SCWD}}, \dots, \bar{C}_{L=I}^{\text{SCWD}} \}. \quad (53)$$

1) *Empirical configuration:* Regarding the empirical configuration, some spatial domain parameters are the same as those used in the SD strategy for a fairer comparison: $\phi_{1/2} = 60^\circ$, $\mathbf{m}_{\text{fov}} = 1.4738$, $\theta_{\text{pd}} = 40^\circ$. The values of x_l and y_l with different number of clusters L are selected based on Fig. 5. The configuration of $\lambda_{c,m}^{\text{led}}, \lambda_{c,m}^{\text{of}}$ and $\Delta\lambda^{\text{of}}$ are similar to (44) and (45) in the WD strategy empirical configuration:

$$\Delta\lambda^{\text{of}} = (\lambda_{\text{max}} - \lambda_{\text{min}}) / \lceil I/L \rceil, \quad (54)$$

$$\lambda_{c,m}^{\text{led}} = \lambda_{c,m}^{\text{of}} = \lambda_{\text{min}} + (m - 0.5)\Delta\lambda^{\text{of}}. \quad (55)$$

After evaluation of \bar{C}_L^{SCWD} for all possible L , the highest achievable rate \bar{C}^{SCWD} is selected using (53).

2) *Configuration with BADS algorithm:* The black-box optimisation problem for SCWD strategy is defined as:

$$\underset{\mathcal{X}}{\text{maximise}} \quad \bar{C}_L^{\text{SCWD}}(\mathcal{X}) \text{ with } \mathcal{X} = \{x_l, y_l, \lambda_{c,m}^{\text{led}}, \lambda_{c,m}^{\text{of}}, \phi_{1/2}, \mathbf{m}_{\text{fov}}, (\theta_{\text{pd}}), \Delta\lambda^{\text{of}}\} \quad (56)$$

$$\text{subject to} \quad 0 < \frac{x_l}{W_{\text{room}}} < 1 \text{ for } l = 1, 2, \dots, L, \quad (57)$$

$$0 < \frac{y_l}{L_{\text{room}}} < 1 \text{ for } l = 1, 2, \dots, L, \quad (58)$$

$$\lambda_{\min} \leq \lambda_{c,m}^{\text{led}} \leq \lambda_{\max} \text{ for } m = 1, 2, \dots, M_l, \quad (59)$$

$$\lambda_{\min} \leq \lambda_{c,m}^{\text{of}} \leq \lambda_{\max} \text{ for } m = 1, 2, \dots, M_l, \quad (60)$$

$$0^\circ < \phi_{1/2} \leq 60^\circ, \quad (61)$$

$$m_{\text{fov}} \geq 1, \quad (62)$$

$$(0^\circ \leq \theta_{\text{pd}} \leq 90^\circ) \quad (63)$$

$$\Delta\lambda^{\text{of}} > 0, \quad (64)$$

Note that solving this problem only finds the highest average achievable rate with L clusters. Therefore, the BADS algorithm need to be executed for I times for each initial solution so that the achievable rates for all possible L are obtained. It is challenging to include the parameter L as one of the optimisation variables, as the number of parameters in the system configuration is a function of L .

Fig. 7 shows the average rates achieved by the joint multiplexing systems with the SCWD strategy against different numbers of elements. In addition, the results with SD and WD strategies are also included for comparison. The remaining parameters are listed in Table II if they are not specified. The four plots show cases with different receiver orientation scenarios and with different types of configurations, respectively. It can be observed that with an increase in the number of elements, the average achievable rate by the SCWD strategy systems also increases consistently, even when the number of elements is greater than 10. With 16 optical elements, the data rates achieved by SCWD systems are in the range of 1300 to 2200 Mbps, while those achieved by either SD or WD systems fall in the range of 500 to 1400 Mbps. The achievable rate improvement is between 36% and 74% compared to the SD strategy, and the improvement is between 47% and 135% compared to the WD strategy. In general, the SCWD systems with PR shows a slightly better performance at a high number of elements compared to those with HR.

G. Insights into the system parameter configurations and SCWD strategy

In this subsection, we will discuss the difference between the parameters used in the empirical configurations and configurations with the BADS algorithm. We will also explain why the SCWD

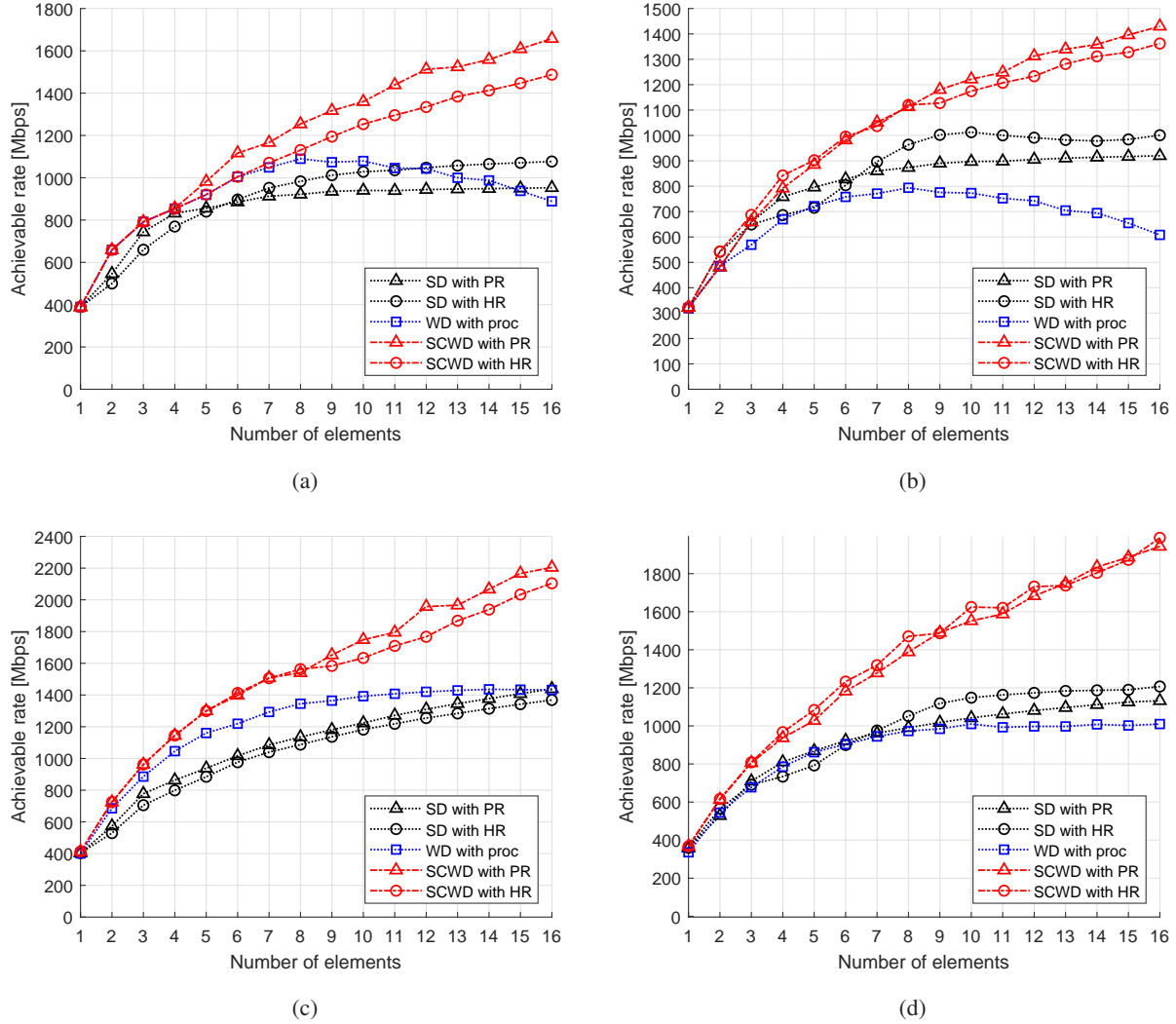


Figure 7: Average achievable rate of joint multiplexing systems with SCWD strategy against number of elements. (a) Empirical configurations with upward receiver orientation. (b) Empirical configurations with random receiver orientation. (c) BADS-based configurations with upward receiver orientation. (d) BADS-based configurations with random receiver orientation.

strategy is able to provide extra multiplexing gains when compared to SD and WD strategies. For simplicity, the cases with a PR and the upward receiver orientation are demonstrated as an example. The comparison between parameters used in empirical and BADS-based configurations with 16 elements is shown in Fig. 8a. In both configurations, there are four spatial clusters, as demonstrated in Fig. 8a 1). Regarding the geometric parameters, the spatial positions of LED clusters are closer to the room centre in the case of BADS-based configuration compared to the empirical configuration. In addition, a smaller half-power semiangle of $\phi_{1/2} = 35.2^\circ$ is used on the transmitter side and a smaller FoV coefficient of $m_{\text{foV}} = 1$ is used on the receiver side

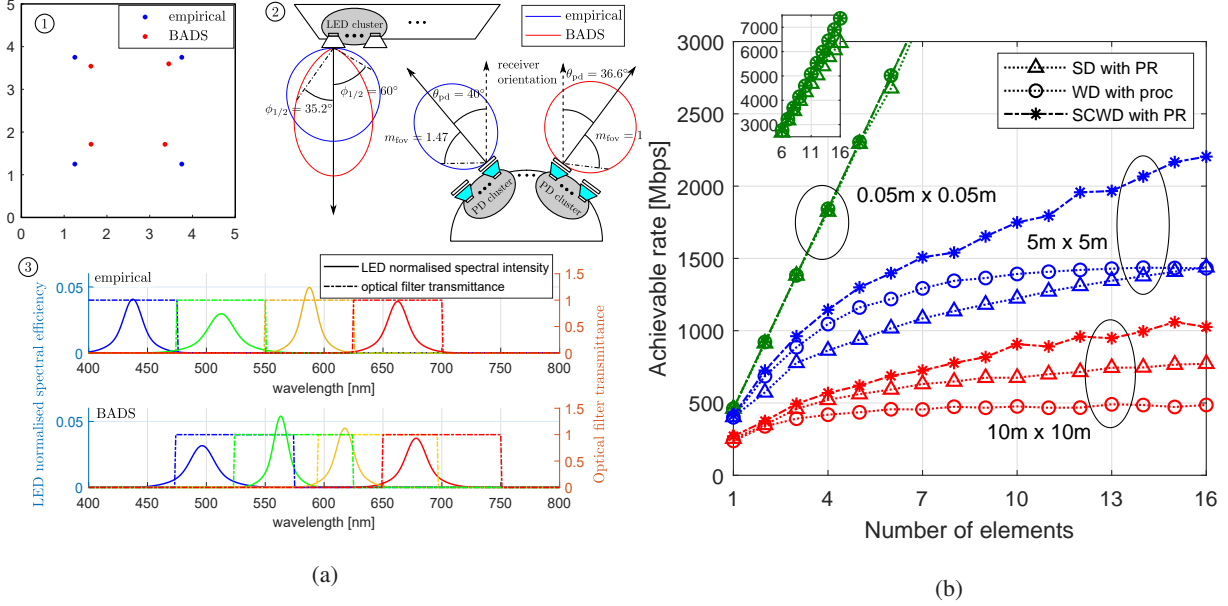


Figure 8: (a) Comparison between empirical and BADS-based configuration parameters used in 16-elements joint multiplexing systems with SCWD strategy. The demonstrated systems use PR and upward receiver orientation scenario. 1) LED cluster position layout. 2) Angular parameters. 3) Wavelength-dependent parameters. (b) Achievable rate of systems using optimised configurations with PR and upward receiver orientation scenario against number of elements in two special conditions. Condition 1: larger room of size 10 m \times 10 m. Condition 2: extremely small space of size 0.05 m \times 0.05 m. Default condition: room size of 5 m \times 5 m.

compared to the empirical configuration, as shown in Fig. 8a 2). These parameter changes lead to weaker spatial channel correlation and thereby achieving higher overall multiplexing gain. Regarding the wavelength domain parameters, four WDs are used within each spatial cluster, as shown in Fig. 8a 3). Compared to the case of empirical configuration, all LED spectra shift to the longer wavelengths with smaller separations in the case of BADS-based configuration. This is because the PD has a higher responsivity at a longer wavelength and the additional inter-colour interference introduced by smaller separation causes negligible distortion. In addition, the passband of optical filters are extended to longer wavelengths in the case of BADS-based configuration, which compensate bandpass shift issue when light incident angle is large.

In order to demonstrate the characteristics of the SCWD strategy, we can evaluate the performance of joint multiplexing systems using BADS-based configurations with PR and upward receiver orientation scenario under several conditions. In addition to cases with normal conditions (i.e. a room size of 5 m \times 5 m \times 3 m) shown in Fig. 7c, we further evaluate two special conditions. In the first condition, we show the transmissions in a large room of size 10 m \times 10 m \times 3 m. The

remaining system parameters are identical to those used in Sections IV-D, IV-E and IV-F. Due to the increase in coverage area, the average link distance becomes greater and the misalignment issue due to random user position and orientation is more severe. These factors lead to a further decrease in the data rate achieved by joint multiplexing systems, as shown in Fig. 8b. The achievable rate decrease is more severe for the case of WD strategy, where random users are more likely to receive a weaker signal as all LEDs are located in the room centre. Therefore, the achievable rate of the WD strategy is considerably lower than the case of SD strategy with the same number of elements. Due to the inferior performance of system with WD strategy, the SCWD strategy provides a decreased achievable rate improvement against its counterparts compared to the case with $5\text{ m} \times 5\text{ m} \times 3\text{ m}$ room. In the second special condition, we show that transmissions in an extremely small indoor space of size $0.05\text{ m} \times 0.05\text{ m} \times 3\text{ m}$. With such a small coverage area and the upward receiver scenario, all users experience a minimised link distance with good alignment. Consequently, the passband shift issue in systems with the WD strategy can be avoided. Note that a half-power semiangle of $\phi_{1/2} = 1.5^\circ$ is also used in the case of WD strategy to maximise the detected optical power. In the case of SD strategy, performance degradation due to greater link distance and misalignment is avoided. In addition, a BADS-based configuration solution with a very collimated light beam and light reception pattern is obtained in case of the SD strategy. Due to all the above factors, the joint multiplexing systems with WD and SD strategies can operate in ideal conditions. Specifically, the multiplexing gain scales almost linearly with the number of elements, as shown in Fig. 8b. In this condition, despite the minor performance gap between WD and SD systems, the multiplexing gain of both systems are approaching the theoretical limit of multiplexing systems. Consequently, the system with SCWD strategy exhibits a similar ideal performance.

Despite the undesired performance exhibited in the two special conditions, using a MIMO VLC system to cover an extremely large or extremely small area is unlikely in practice. As long as the following two conditions are fulfilled, SCWD strategy will provide a considerable improvement: 1) there is a minor performance gap between joint multiplexing systems with SD and WD strategies, 2) multiplexing transmissions in individual spatial and wavelength domains are inefficient. In general conditions of where a medium sized room is covered, similar achievable rates are likely to be achieved by systems with SD and WD strategies. In addition, the efficiency of VLC multiplexing systems is limited by the random user position/orientation and channel correlation. Therefore, the SCWD strategy is likely to provide a remarkable achievable rate

improvement, as shown in Fig. 7. The configuration problem in joint multiplexing systems is similar to a power allocation problem in a multi-carrier transmission system with two channels. If both channels have similar qualities, loading them with power leads to a higher performance compared to loading all the power to one channel. However, if one of the channels is unreliable or the spectral efficiency scales linearly with the power increase, loading two channels will no longer be beneficial.

H. Practical implementation and illumination

For implementations of the VLC MIMO joint multiplexing system with the proposed SCWD strategy, there are several practical solutions. For example, it is challenging to mount more than ten PDs on the same side of a portable device, while it is easier to mount a cluster of a few PDs on each side of a device with a different orientation [27]. For small devices, such as smart phones, mounting one or two PDs on each side of the device is realistic. The system with a greater number of PDs can be implemented on larger devices such as tablets, laptop or Internet-of-things (IoT) device. On the transmitter side, the SCWD strategy gather multiple LEDs with different wavelengths in the same cluster. This feature provides an opportunity to generate white light illumination by manipulating the intensity ratio of LEDs with different colours [40]. In the cases where the LEDs in the cluster are insufficient to provide the desired white light, additional LEDs with suitable wavelengths can be installed in the LED cluster so that the combined light reaches the illumination requirement.

V. CONCLUSIONS

A framework for a VLC MIMO-OFDM joint multiplexing system with a channel dependent on spatial, wavelength and frequency domain characteristics is proposed. This study focused on investigating the suitable system configurations for the VLC joint multiplexing system with different strategies in order to achieve a higher multiplexing gain, thereby achieving a higher aggregate transmission data rate. The proposed SCWD strategy shows a considerable improvement in the average achievable rate compared to cases with SD and WD strategies. The use of the BADS black-box optimisation algorithm improves the achievable rates further. The simulation results demonstrate an average achievable rate improvement of 36% to 135% with 16 LEDs/PDs by using the proposed SCWD strategy compared to those achieved with SD and WD strategies. This work also demonstrated the possibility of using a VLC MIMO-OFDM system with limited

modulation bandwidth to achieve multi-Gbps transmission data rates, which shows the potential of VLC/LiFi systems in next generation wireless networks in terms of achievable rate capability. In future studies, the scenarios with multiple access or multi-user MIMO will be investigated.

REFERENCES

- [1] W. Jiang, B. Han, M. A. Habibi, and H. D. Schotten, "The Road Towards 6G: A Comprehensive Survey," *IEEE Open Journal of the Communications Society*, vol. 2, pp. 334–366, 2021.
- [2] H. Haas, L. Yin, Y. Wang, and C. Chen, "What is LiFi?" *J. Lightw. Technol.*, vol. 34, no. 6, pp. 1533–1544, Mar. 2016.
- [3] J. Raring, C. Lee, M. S. Islam, A. Sparks, S. Videv, M. McLaurin, B. Shah, P. Rudy, and H. Haas, ">25 Gbit/s LiFi with Laser Based SMD White Light Source," in *Optical Fiber Communications Conference and Exhibition*, 2021, pp. 1–3.
- [4] E. Xie, R. Bian, X. He, M. S. Islam, C. Chen, J. J. D. McKendry, E. Gu, H. Haas, and M. D. Dawson, "Over 10 gbps vlc for long-distance applications using a gan-based series-biased micro-led array," *IEEE Photonics Technology Letters*, vol. 32, no. 9, pp. 499–502, 2020.
- [5] T. Fath and H. Haas, "Performance comparison of mimo techniques for optical wireless communications in indoor environments," *IEEE Trans. Commun.*, vol. 61, no. 2, pp. 733–742, February 2013.
- [6] K. Ying, H. Qian, R. J. Baxley, and S. Yao, "Joint optimization of precoder and equalizer in mimo vlc systems," *IEEE J. Sel. Areas Commun.*, vol. 33, no. 9, pp. 1949–1958, Sep. 2015.
- [7] P. M. Butala, H. Elgala, and T. D. C. Little, "SVD-VLC: A Novel Capacity Maximizing VLC MIMO System Architecture Under Illumination Constraints," in *2013 IEEE Globecom Workshops (GC Wkshps)*, 2013, pp. 1087–1092.
- [8] Y. Hong, T. Wu, and L.-K. Chen, "On the Performance of Adaptive MIMO-OFDM Indoor Visible Light Communications," *IEEE Photonics Technology Letters*, vol. 28, no. 8, pp. 907–910, 2016.
- [9] C. He, T. Q. Wang, and J. Armstrong, "Performance Comparison between Spatial Multiplexing and Spatial Modulation in Indoor MIMO Visible Light Communication Systems," in *IEEE International Conf. on Commun.*, 2016, pp. 1–6.
- [10] Y. Tan and H. Haas, "Coherent LiFi System With Spatial Multiplexing," *IEEE Transactions on Communications*, vol. 69, no. 7, pp. 4632–4643, 2021.
- [11] R. Bian, I. Tavakkolnia, and H. Haas, "15.73 Gb/s Visible Light Communication With Off-the-Shelf LEDs," *Journal of Lightwave Technology*, vol. 37, no. 10, pp. 2418–2424, 2019.
- [12] G. Cossu, A. Khalid, P. Choudhury, R. Corsini, and E. Ciaramella, "3.4 Gbit/s Visible Optical Wireless Transmission based on RGB LED," *Optics Express*, vol. 20, no. 26, pp. B501–B506, 2012.
- [13] L. Cui, Y. Tang, H. Jia, J. Luo, and B. Gnade, "Analysis of the Multichannel WDM-VLC Communication System," *Journal of Lightwave Technology*, vol. 34, no. 24, pp. 5627–5634, 2016.
- [14] N. Omura, A. Higashi, J. Yabuuchi, T. Iwamatsu, and S. Oshiba, "Experimental Demonstration of OFDM Based WDM-MIMO Visible Light Communication System," in *2018 Asia-Pacific Microwave Conference (APMC)*, 2018, pp. 872–874.
- [15] H. Lee, I. Lee, and S. H. Lee, "Deep Learning based Transceiver Design for Multi-Colored VLC Systems," *Optics Express*, vol. 26, no. 5, pp. 6222–6238, 2018.
- [16] A. Burton, P. Chvojka, P. A. Haigh, Z. Ghassemlooy, and S. Zvanovec, "Optical Filter-Less WDM for Visible Light Communications Using Defocused MIMO," *Electronics*, vol. 10, no. 9, p. 1065, 2021.
- [17] R. Wang, Q. Gao, J. You, E. Liu, P. Wang, Z. Xu, and Y. Hua, "Linear Transceiver Designs for MIMO Indoor Visible Light Communications Under Lighting Constraints," *IEEE Trans. Commun.*, vol. 65, no. 6, pp. 2494–2508, 2017.
- [18] Y. Xiao and Y.-J. Zhu, "Chromaticity-Adaptive Generalized Spatial Modulation for MIMO VLC With Multi-Color LEDs," *IEEE Photonics Journal*, vol. 11, no. 4, pp. 1–12, 2019.

- [19] R. Sharma, A. C. Kumari, M. Aggarwal, and S. Ahuja, "Optimal LED Deployment for Mobile Indoor Visible Light Communication System: Performance Analysis," *AEU-International Journal of Electronics and Communications*, vol. 83, pp. 427–432, 2018.
- [20] M. T. Niaz, F. Imdad, S. Kim, and H. S. Kim, "Deployment Methods of Visible Light Communication Lights for Energy Efficient Buildings," *Optical Engineering*, vol. 55, no. 10, p. 106113, 2016.
- [21] M. S. Gismalla, M. F. L. Abdullah, M. S. Ahmed, W. A. Mabrouk, A.-F. Najib, E. Saeid, A. Supa'at, and B. Das, "Design and Analysis of Different Optical Attocells Deployment Models for Indoor Visible Light Communication System," *International Journal of Integrated Engineering*, vol. 13, no. 6, pp. 253–264, 2021.
- [22] J. Xu, C. Gong, J. Luo, and Z. Xu, "LED Half-Power Angle Optimization for Ultra-Dense Indoor Visible Light Communication Network Deployment," *IEEE Open Journal of the Communications Society*, vol. 1, pp. 835–848, 2020.
- [23] A. Nuwanpriya, S. W. Ho, and C. S. Chen, "Indoor MIMO Visible Light Communications: Novel Angle Diversity Receivers for Mobile Users," *IEEE J. Sel. Areas Commun.*, vol. 33, no. 9, pp. 1780–1792, Sep. 2015.
- [24] K.-H. Park, W. G. Alheadary, and M.-S. Alouini, "A Novel Mirror Diversity Receiver for Indoor MIMO Visible Light Communication Systems," in *2016 IEEE 27th Annual International Symposium on Personal, Indoor, and Mobile Radio Communications (PIMRC)*, 2016, pp. 1–6.
- [25] A. A. Purwita, A. Yesilkaya, I. Tavakkolnia, M. Safari, and H. Haas, "Effects of Irregular Photodiode Configurations for Indoor MIMO VLC with Mobile Users," in *2019 IEEE 30th Annual International Symposium on Personal, Indoor and Mobile Radio Communications (PIMRC)*, 2019, pp. 1–7.
- [26] P. Ge, X. Liang, J. Wang, C. Zhao, X. Gao, and Z. Ding, "Optical Filter Designs for Multi-Color Visible Light Communication," *IEEE Transactions on Communications*, vol. 67, no. 3, pp. 2173–2187, 2019.
- [27] C. Chen, I. Tavakkolnia, M. D. Soltani, M. Safari, and H. Haas, "Hybrid Multiplexing in OFDM-based VLC Systems," in *2020 IEEE Wireless Communications and Networking Conference (WCNC)*, 2020, pp. 1–6.
- [28] D. Tsonev, S. Sinanovic, and H. Haas, "Complete Modeling of Nonlinear Distortion in OFDM-based Optical Wireless Communication," *J. Lightw. Technol.*, vol. 31, no. 18, pp. 3064–3076, Sep. 15 2013.
- [29] S. Dimitrov, S. Sinanovic, and H. Haas, "Clipping Noise in OFDM-Based Optical Wireless Communication Systems," *IEEE Trans. Commun.*, vol. 60, no. 4, pp. 1072–1081, Apr. 2012.
- [30] H. Schulze, "Frequency-Domain Simulation of the Indoor Wireless Optical Communication Channel," *IEEE Trans. Commun.*, vol. 64, no. 6, pp. 2551–2562, June 2016.
- [31] J. Barry, J. Kahn, W. Krause, E. Lee, and D. Messerschmitt, "Simulation of Multipath Impulse Response for Indoor Wireless Optical Channels," *IEEE J. Sel. Areas Commun.*, vol. 11, no. 3, pp. 367–379, Apr. 1993.
- [32] S. Hranilovic, *Wireless Optical Communication Systems*. Springer Science & Business Media, 2006.
- [33] T. E. B. Cunha, J.-P. M. G. Linnartz, and X. Deng, "Achievable Rate of LED-based Distributed MIMO OWC Systems Under a Per-LED Power Constraint," in *2021 17th International Symposium on Wireless Communication Systems (ISWCS)*, 2021, pp. 1–6.
- [34] M. D. Soltani, M. A. Arfaoui, I. Tavakkolnia, A. Ghayeb, M. Safari, C. M. Assi, M. O. Hasna, and H. Haas, "Bidirectional Optical Spatial Modulation for Mobile Users: Toward a Practical Design for LiFi Systems," *IEEE Journal on Selected Areas in Communications*, vol. 37, no. 9, pp. 2069–2086, 2019.
- [35] C. Audet and W. Hare, *Derivative-free and Blackbox Optimization*. Springer, 2017, vol. 2.
- [36] L. Acerbi and W. J. Ma, "Practical Bayesian Optimization for Model Fitting with Bayesian Adaptive Direct Search," in *Proceedings of the 31st International Conference on Neural Information Processing Systems*, 2017, pp. 1834–1844.
- [37] J.-A. Li, D. Dong, Z. Wei, Y. Liu, Y. Pan, F. Nori, and X. Zhang, "Quantum Reinforcement Learning During Human Decision-Making," *Nature human behaviour*, vol. 4, no. 3, pp. 294–307, 2020.

- [38] C. Audet and J. E. Dennis Jr, “Mesh Adaptive Direct Search Algorithms for Constrained Optimization,” *SIAM Journal on optimization*, vol. 17, no. 1, pp. 188–217, 2006.
- [39] S. Mardanikorani, X. Deng, and J.-P. M. G. Linnartz, “Sub-Carrier Loading Strategies for DCO-OFDM LED Communication,” *IEEE Transactions on Communications*, vol. 68, no. 2, pp. 1101–1117, 2020.
- [40] C. Gong, S. Li, Q. Gao, and Z. Xu, “Power and Rate Optimization for Visible Light Communication System With Lighting Constraints,” *IEEE Transactions on Signal Processing*, vol. 63, no. 16, pp. 4245–4256, 2015.